

**Bound states in ultrastrong waveguide QED**Juan Román-Roche<sup>1</sup>, Eduardo Sánchez-Burillo<sup>2</sup> and David Zueco<sup>1,3</sup><sup>1</sup>*Instituto de Nanociencia y Materiales de Aragón (INMA) and Departamento de Física de la Materia Condensada, CSIC-Universidad de Zaragoza, Zaragoza 50009, Spain*<sup>2</sup>*Max-Planck-Institut für Quantenoptik, D-85748 Garching, Germany*<sup>3</sup>*Fundación ARAID, Campus Río Ebro, 50018 Zaragoza, Spain*

(Received 15 February 2020; accepted 10 July 2020; published 3 August 2020)

We discuss the properties of bound states in finite-bandwidth waveguide QED beyond the rotating wave approximation or excitation-number-conserving light-matter coupling models. Therefore, we extend the *standard* calculations to a broader range of light-matter strengths, in particular, in the so-called ultrastrong coupling regime. We do this using the polaron technique. Our main results are as follows: We compute the spontaneous emission rate, which is renormalized as compared with the Fermi golden rule formula. We generalize the existence criteria for bound states, their properties, and their role in the qubit thermalization. We discuss effective spin-spin interactions through both vacuum fluctuations and bound states. Finally, we sketch a perfect state-transfer protocol among distant emitters mediated by bound states.

DOI: [10.1103/PhysRevA.102.023702](https://doi.org/10.1103/PhysRevA.102.023702)**I. INTRODUCTION**

Photons are weakly coupled to matter, so they rarely interact, making them perfect information carriers. Weak coupling constitutes, however, a double-edged sword, as it also hinders the readout process when the time comes to access the information being carried. The trade-off is optimized in waveguide QED, where the photons are confined in one-dimensional waveguides to enhance the light-matter coupling [1,2]. So far, different experimental platforms have been used to implement this coupling between quantum emitters (typically two-level systems or qubits) and a one-dimensional quantized electromagnetic field. Examples are superconducting circuits [3–5] and optical waveguides [6], among others [7,8]. Waveguide QED can serve to control light-matter emission, to induce photon-photon interactions, or to route the photons in quantum networks. Besides, by engineering the guides, more exotic interfaces can be implemented for quantum simulation [9], topological photonics [10], chirality [11,12], or quantum computing [13]. Consequently, waveguide QED may be a quantum technological solution.

Trying to optimize the light-matter coupling, several experiments have reached the so-called ultrastrong coupling regime (USC) between light and a single quantum emitter, both in cavity [14,15] and waveguide QED [16–18]. The USC is the regime where higher-order processes than the creation (annihilation) of *one* photon by annihilating (creating) *one* matter excitation play a role. Two main phenomena are paradigmatic of USC. The rotating wave approximation (RWA) for the interaction breaks down and the atomic bare parameters get renormalized, either the Bloch-Siegert shift [19] in cavity QED or the renormalization due to the coupling to the continuum electromagnetic (EM) field in waveguide QED [20]. Besides, the ground state becomes nontrivial [21]. This has interesting consequences. Some of them are

the possibility of transforming virtual into real photons by perturbing the ground state [22–25], doing nonlinear optics with zero photons [26]. Further phenomenology in cavity QED can be found in recent reviews [27,28]. In this work we are interested in the USC regime in waveguide QED. Apart from the qubit frequency renormalization, there exist the localization-delocalization transition [29,30], particle production [31], nonlinear optics at the single-photon limit [32,33], and vacuum light emission [34].

In *conventional* waveguide QED, i.e., when the RWA can be performed, the main objective is to control atom-atom interactions mediated by the waveguide's EM-fluctuations [35–39]. Propagating photons induce long-range but dissipative interactions. Dissipative because the information is lost in the traveling wave packets. On the other hand, dressed atom-field eigenstates localized around the quantum emitter, called bound states [40–44], generate nondissipative but exponentially bounded interactions [10,12,45–54].

These exact nonpropagating eigenstates lie within the band gap (hence *nonpropagating*). Besides, bound states modify the spontaneous emission [55–64], which makes them an interesting resource for engineering quantum photonics.

In *this work*, we discuss the physics of bound states in the USC regime of waveguide QED. We focus on the lowest-energy ones, discussing their existence and role in the spontaneous emission and thermalization. We also discuss the effective spin-spin models emerging when several emitters are ultrastrongly coupled to the EM field and envision protocols for perfect state transfer between distant atoms. To do this, we face a technical difficulty. The light-matter coupling is modeled via spin-boson-type Hamiltonians, a paradigmatic example of a nonexactly solvable model [65]. Different techniques are available in the literature to deal with it. Matrix-product states (MPSs) [29,32,33], density matrix renormalization group (DMRG) [66], and path integral

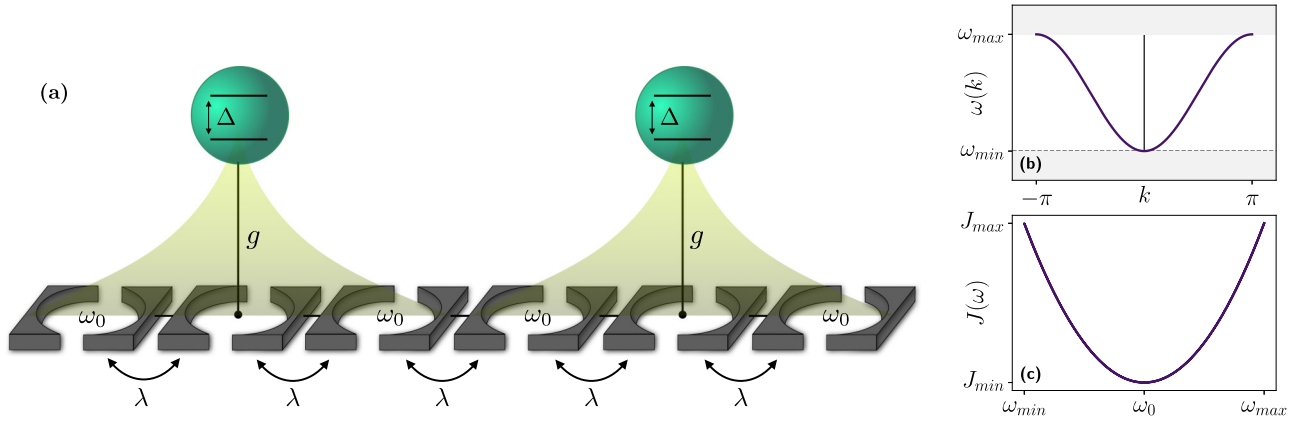


FIG. 1. (a) Schematic depiction of two qubits coupled to specific sites of a linear cavity array, where  $g$  is the coupling constant,  $\Delta$  is the energy difference between the two states of the qubits,  $\omega_0$  is the resonance frequency for photons in the cavity (omitted in the coupled cavities for aesthetic purposes), and  $\lambda$  is the hopping constant for photons traveling between cavities. The yellow shades represent localized-photon clouds. (b) Finite-band dispersion relation of the model. (c) Spectral density function for the model.

approaches [67,68] comprise the toolbox of numerical techniques. Analytical treatments are also used. They are based on different variational *Ansätze*: polaron-like [30,34,69–72] or Gaussian ones [73]. In this paper we use a polaron-type approach that has been shown to be accurate over a wide range of parameters, including couplings well inside the USC.

The rest of the paper is organized as follows: In the next section, Sec. II, we will introduce the system, its model and the polaron picture. In Sec. III, we treat the single-emitter case. We discuss the ground-state properties and the lowest bound state, discussing its existence conditions, energy, localization length, and spontaneous emission. Section IV develops the multiqubit case with emphasis in the effective tight-binding model and in protocols for perfect state transfer. We finish with some conclusions. Several technical issues are sent to the Appendixes. Finally, the link to the python codes used in the numerical calculations is given in Appendix D.

## II. LIGHT-MATTER INTERACTION AND THE POLARON PICTURE

### A. Model

In this paper we study the system sketched in Fig. 1(a). Several qubits are coupled to a cavity array forming the photonic medium. In the dipole gauge [74] and assuming that each qubit is coupled to a single cavity, the model is ( $\hbar = 1$  is set through the paper)

$$H = \sum_{j=1}^{N_q} \frac{\Delta}{2} \sigma_j^z + \omega_0 \sum_n^N b_n^\dagger b_n - \lambda \sum_n^N (b_n^\dagger b_{n-1} + \text{H.c.}) + g \sum_{j=1}^{N_q} \sigma_j^x (b_{x_j}^\dagger + b_{x_j}). \quad (1)$$

Here,  $N_q$  is the total number of qubits with level splitting  $\Delta$  (let us assume that all the atoms are identical).  $N$  is the number of sites; we consider the thermodynamic limit  $N \rightarrow \infty$  in our analytical treatment.  $x_j$  is the site to which the  $j$ th qubit is coupled. Operators  $b_n^\dagger$  and  $b_n$  correspond to the bosonic

creation and annihilation operators at site  $n$ , and  $\sigma^z$  and  $\sigma^x$  are the  $z$  and  $x$  Pauli matrices. To avoid extra parameters, we consider that the qubit-resonator coupling is the same for all the qubits,  $g$ . The photonic medium [second and third terms in Eq. (1)], which is a cavity array, is diagonalized by introducing the bosonic operators in momentum space, which are the Fourier transform of their spatial counterparts:  $b_k = \frac{1}{\sqrt{N}} \sum_n e^{ikn} b_n$ , obtaining

$$H = \frac{\Delta}{2} \sum_{j=1}^{N_q} \sigma_j^z + \sum_k \omega_k b_k^\dagger b_k + \sum_{j=1}^{N_q} \sigma_j^x \sum_k c_k (b_k^\dagger e^{ikx_j} + b_k e^{-ikx_j}). \quad (2)$$

The dispersion relation sketched in Fig. 1(b) is

$$\omega_k = \omega_0 - 2\lambda \cos k, \quad (3)$$

and the coupling per spin in momentum space is given by

$$c_k = \frac{g}{\sqrt{N}}. \quad (4)$$

The dispersion relation is a finite band of width  $4\lambda$  centered around  $\omega_0$ . Besides, the coupling constant is independent of the photonic mode and proportional to  $g$ , which justifies why, throughout this work, we refer to both  $g$  and  $c_k$  indistinctly as the *coupling constant*. Finally, it is convenient to define the spectral density, plotted in Fig. 1(c),

$$J(\omega) = 2\pi \sum_k |c_k|^2 \delta(\omega - \omega_k), \quad (5)$$

conveniently rewritten in terms of the density of states:<sup>1</sup>

$$J(\omega) = 2\pi g^2 \left( \frac{d\omega_k}{dk} \right)^{-1}. \quad (6)$$

<sup>1</sup>Take a function  $f(\omega)$ . Then,  $\int d\omega J(\omega) f(\omega) = 2\pi g / \sqrt{N} \sum_k f(\omega_k) \rightarrow 2\pi g \int d\omega (d\omega_k/dk)^{-1} f(\omega)$ . This yields Eq. (6) in the main text.

### B. A brief comment on the rotating wave approximation

If the coupling constant is small enough, the rotating wave approximation can be used, by which the interaction term [last term in Eq. (1)] becomes

$$\sum_{j=1}^{N_q} \sum_k c_k (\sigma_j^- b_k^\dagger + \sigma_j^+ b_k). \quad (7)$$

It is clear now that the state  $|0_1, 0_2, \dots, 0_{N_q}; \mathbf{0}\rangle$  with  $\sigma_j^z |0_j\rangle = -|0_j\rangle$  and  $b_k |0\rangle = 0$  is the (trivial) ground state (GS) of the system and that the Hamiltonian preserves the number of excitations  $N$ ,  $[H, N] = 0$  with  $N = \sum_k b_k^\dagger b_k + \sum_{j=1}^{N_q} \sigma_j^+ \sigma_j^-$ . Consequently, within the RWA, the dynamics are split in subspaces with a fixed number of excitations which makes the low-energy dynamics amenable, at least numerically.

### C. Polaron picture

It has been shown that the low-energy sector, i.e., the ground state and some excited states, of a spin-boson model (2) is well approximated by an effective, excitation-number-conserving Hamiltonian derived from a polaron transformation [70,71]. The basic idea is to construct a unitary transformation that disentangles the two level system (TLS) from the bath. This unitary transformation depends on some parameters that are found with the variational principle. In this case, the *Ansatz* is

$$|\Psi_{\text{GS}}[\tilde{f}_k, \zeta_s]\rangle = U_P[\tilde{f}_k] |\mathbf{0}\rangle \otimes \sum_{s_j=0,1} \zeta_s |s_1, \dots, s_{N_q}\rangle. \quad (8)$$

Here  $|\mathbf{0}\rangle$  is the photon vacuum state ( $b_k |\mathbf{0}\rangle = 0$  for all  $k$ ) and the spin state is arbitrary. The variational parameters are the  $\zeta_s$  coefficients and  $\{\tilde{f}_k\}$ , the  $N$  parameters in the unitary  $U_P$ . Building up on previous work from McCutcheon *et al.* [75] and Zheng *et al.* [76] we used a natural extension of the single-qubit polaron transform (PT) valid for arbitrarily distant qubits:

$$U_P = \exp \left[ - \sum_{j=1}^{N_q} \sigma_j^x \sum_k (\tilde{f}_k b_k^\dagger e^{ikx_j} - \tilde{f}_k^* b_k e^{-ikx_j}) \right]. \quad (9)$$

The parameters  $\{\tilde{f}_k\}$  are hereinafter assumed to be real without loss of generality, since the complex phase can be absorbed by the bosonic operators while preserving canonical commutation. Provided there is no privileged direction of travel, we can assume that, for each boson with wave number  $k$ , there will be another with  $-k$ , so that  $|\tilde{f}_k| = |\tilde{f}_{-k}|$ . From that, and the fact that the sine function is odd, Eq. (9) factors as

$$U_P = \bigotimes_{j=1}^{N_q} U_j, \quad (10)$$

with

$$U_j = \exp \left[ - \sigma_j^x \sum_k \tilde{f}_k (b_k^\dagger e^{ikx_j} - b_k e^{-ikx_j}) \right].$$

It turns out that minimizing the energy of the spin-boson (2),

$$\epsilon_{\text{GS}} = \min_{\tilde{f}_k, \zeta_s} \{ \langle \Psi_{\text{GS}}[\tilde{f}_k, \zeta_s] | H | \Psi_{\text{GS}}[\tilde{f}_k, \zeta_s] \rangle \} \quad (11)$$

is done by finding the ground state of the *effective* spin model

$$\mathcal{H}_S = \frac{\Delta_r}{2} \sum_{j=1}^{N_q} \sigma_j^z + \sum_{i<j} \mathcal{J}_{ij} \sigma_i^x \sigma_j^x + N_q \sum_k \tilde{f}_k (\omega_k \tilde{f}_k - 2c_k), \quad (12)$$

with

$$\mathcal{J}_{ij} = 2 \sum_k \tilde{f}_k (2c_k - \omega_k \tilde{f}_k) \cos[k(x_i - x_j)], \quad (13)$$

and the renormalized qubit frequency

$$\Delta_r = \Delta \exp \left[ -2 \sum_k \tilde{f}_k^2 \right]. \quad (14)$$

In the next section we work with explicit expressions in the case of one and two qubits. A generalized polaron transformation is discussed in Appendix C, where it is shown that the much less cumbersome Eq. (9) is sufficient.

## III. SINGLE-QUBIT CASE

In the single-qubit case  $N_q = 1$ , Hamiltonian (2) is nothing but the spin-boson model (see Refs. [20] and [65, Chap. 3]). In this section, we tackle the ground-state properties, the single-qubit bound states, and the spontaneous emission within the USC regime for the cavity array model [Eq. (6)].

### A. Ground state

Setting  $N_q = 1$ , Eqs. (11) and (12) indicate that the minimum of the energy is reached when  $\sigma_z |s_1\rangle = -|s_1\rangle$  [cf. Eq. (12)] with

$$\bar{E}_{\text{GS}} = -\frac{\Delta_r}{2} + \sum_k \omega_k \tilde{f}_k^2 - 2 \sum_k c_k \tilde{f}_k, \quad (15)$$

which is minimum when [69]

$$\tilde{f}_k = \frac{c_k}{\Delta_r + \omega_k}. \quad (16)$$

Putting together Eqs. (14) and (16), we realize that the qubit frequency renormalizes to zero as the coupling strength increases. This is a well-known result [20]. Besides, this renormalization is responsible for the localization-delocalization phase transition that corresponds to the ferromagnetic-antiferromagnetic phase transition in the Kondo model [77]. The delocalized phase corresponds to  $\Delta_r \rightarrow 0$ , then the qubit state can be in either the symmetric or antisymmetric superpositions of the eigenstates of  $\sigma^z$ . On the other hand, if  $c_k = 0$ , the spin is at an eigenstate of  $\sigma^z$ , which corresponds to the localized sector. Note that, in condensed-matter physics, the spin-boson is paradigmatic in impurity models. In those formulations that naturally lead to a double-well interpretation of the TLS, the roles of  $\sigma^x$  and  $\sigma^z$  are switched in the Hamiltonian. In that case,  $c_k = 0$  is viewed as the delocalized regime whereas  $\Delta = 0$  is viewed as the localized regime. By using Eqs. (5) and (16), we can rewrite Eq. (14) as

$$\Delta_r = \Delta \exp \left[ -\frac{1}{\pi} \int d\omega \frac{J(\omega)}{(\Delta_r + \omega)^2} \right]. \quad (17)$$

Having a phase transition depends on  $J(\omega)$  [78]. In our system it is not expected to have critical behavior [79]. It is not within

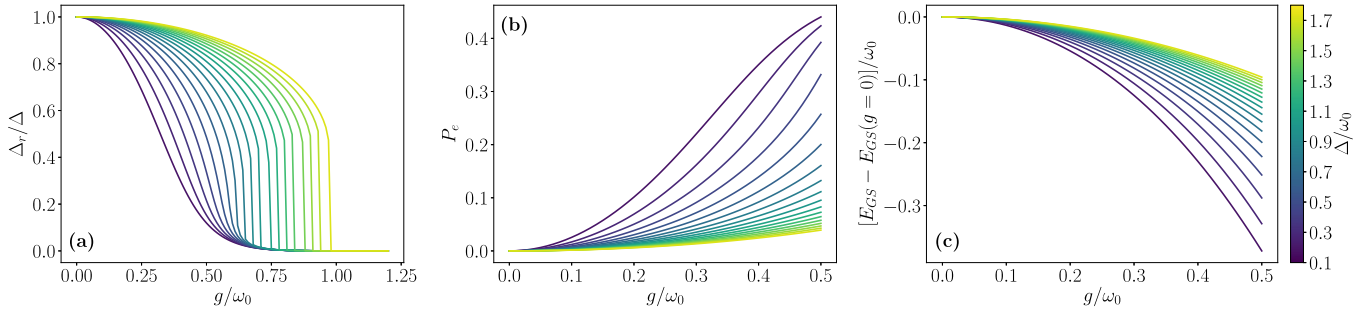


FIG. 2. (a) Renormalized frequency in units of the bare qubit frequency as a function of  $g$  for several values of  $\Delta$ . (b)  $P_e$  as a function of  $g$  for several values of  $\Delta$ . (c) Dependence of the ground-state energy on  $g$  for several values of  $\Delta$ , plotted with respect to the GS energy of an uncoupled qubit and the bath.

the aspirations of this work to study (the absence of) this phase transition, partly because it is not clear that the PT is valid in these ranges, so we will restrict our study to the so-called *ultrastrong coupling* region,  $g \in (0, \approx 0.5)$  in units of  $\omega_0$ , where we are confident that the polaron *Ansatz* works [34,72]. Note that, hereinafter,  $\omega_0$  will be set to 1. As we can see from Fig. 2(a), this region is characterized by a significant, albeit not complete, shrinkage of the tunneling frequency  $\Delta$ , and as such we expect predictions from RWA to fail.

We can further characterize the GS by computing spin observables as in  $P_e = \langle \sigma^+ \sigma^- \rangle$ , the probability of having the spin excited. This is an insightful observable because it relates a measurable quantity  $P_e$  to the renormalized frequency  $\Delta_r$ :

$$P_e = \langle \text{GS} | \sigma^+ \sigma^- | \text{GS} \rangle = \frac{1}{2} \left( 1 - \frac{\Delta_r}{\Delta} \right). \quad (18)$$

Here we used  $\sigma^+ \sigma^- = \frac{1}{2}(\sigma^z + I)$  together with  $\langle \text{GS} | \sigma^z | \text{GS} \rangle = \langle 0 | U_P^\dagger \sigma^z U_P | 0 \rangle = -\frac{\Delta_r}{\Delta}$ . In Fig. 2(b) we show the dependence of  $P_e$  with  $\Delta$  and  $g$ , and alongside is the GS energy plotted in the same parameter range in Fig. 2(c). These are signatures of RWA failure, since within the RWA both  $P_e$  and  $E_{\text{GS}}$  are zero.

Another interesting observable is the spatial distribution of the photons,  $\langle b_n^\dagger b_n \rangle$ . Some algebra (fully done in Appendix A 2) yields

$$\langle b_n^\dagger b_n \rangle = f_n^2, \quad (19)$$

with  $f_n = \frac{1}{\sqrt{N}} \sum_k e^{ik(n-N/2)} \tilde{f}_k$  being the Fourier transform of  $\tilde{f}_k$ . We center the transformation at the qubit position that is understood to be at the middle of the chain. Notice that  $f_n$  has the clear interpretation of being the real-space variational amplitudes for the polaron transformation. Figure 3 shows the spatial distribution of photons as calculated in Eq. (19). We observe that they are well localized around the impurity, exhibiting exponential decay  $f_n \sim \exp\{-\kappa_{\text{GS}}(n - N/2)\}$  with localization length (see Appendix A 3 for a proof)

$$\kappa_{\text{GS}}^{-1} = \text{arccosh}^{-1} \left( \frac{\omega_0 + \Delta_r}{2\lambda} \right). \quad (20)$$

The photons dressing the impurity are commonly named *virtual photons* in reference to their special properties of being nonpropagating and exponentially localized that distinguish them from real photons [80, Chap. 1.3]. Again, this is an effect

of being in the USC regime and is in stark contrast with the GS found with the RWA, which is trivially  $|0_1; \mathbf{0}\rangle$ .

### B. Bound states

We discuss now the single-excitation bound states (SEBSs), which are the basis for creating effective interactions between the qubits. Before moving to the USC regime, let us summarize the existence of bound states within the RWA where the number of excitations is conserved, see Sec. II B. In this case, the lowest-energy bound states are localized eigenstates in the single-excitation subspace. Its energy must be outside of the single-photon band. Given a general photonic model, its existence is not guaranteed; i.e., the eigenvalue equation may not have solutions for energies outside of the dispersion relation [47,59]. Notice that photons in these states cannot propagate. They can be thought of as particles trying to enter a potential barrier greater than their energy and, as such, their wave function must be exponentially decaying with distance from the qubit. It turns out that, within the RWA, Hamiltonian (1) or (2) always accepts two exponentially localized eigenstates: one with energies above and the other below the photonic band.

In the full model (2), the number of excitations is not conserved and we cannot work in the single-excitation subspace. On the other hand, in the polaron picture the effective Hamiltonian  $H_P = U_P^\dagger H U_P$  is approximately number

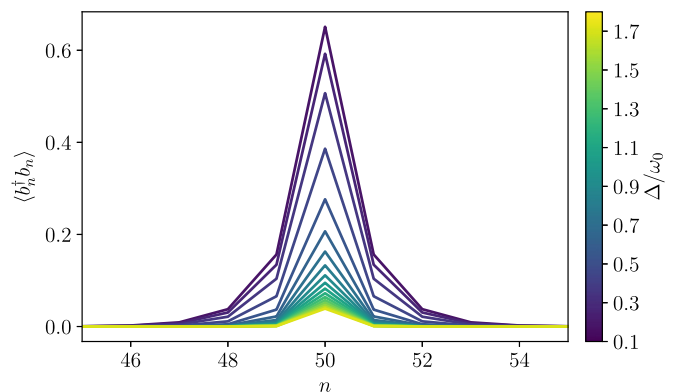


FIG. 3. Comparison of the spatial distribution of GS photons for  $g = 0.5$ .

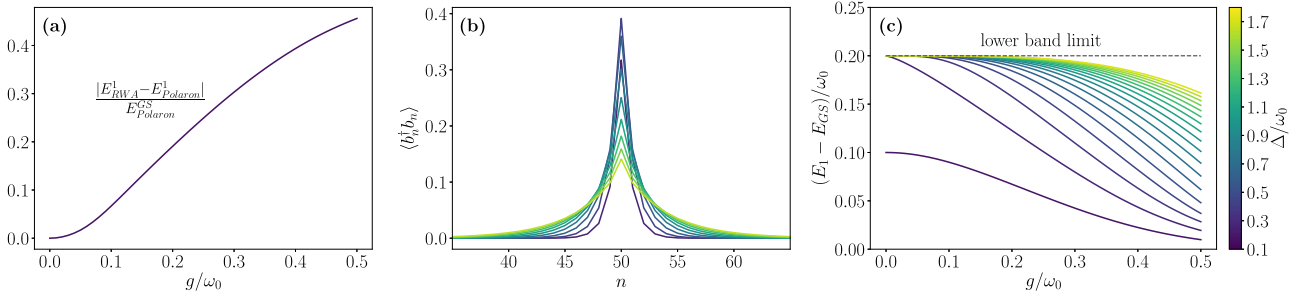


FIG. 4. (a) Relative energy difference between the SEBS as predicted by the PT ( $E_{\text{polaron}}^1$ ) and the RWA ( $E_{\text{RWA}}^1$ ). The ground-state energy is the one calculated with the PT for  $\Delta = 0.3$ . (b) Spatial distribution of photons for  $g = 0.3$  as a function of  $\Delta$ . (c) Energy difference between the first-excited state and the ground state in comparison with the lower band limit as a function of  $g$  and  $\Delta$ .

conserving (see Appendix A 4 for details on the derivation),

$$H_P = \Delta_r \sigma^+ \sigma^- + \sum_k \omega_k b_k^\dagger b_k + 2\Delta_r \left( \sigma^+ \sum_k \tilde{f}_k b_k + \text{H.c.} \right) - 2\Delta_r \sigma_z \sum_{k,p} \tilde{f}_k \tilde{f}_p b_p^\dagger b_p + E_{ZP} + \text{h.o.t.} \quad (21)$$

Here, ‘‘h.o.t.’’ stands for ‘‘higher-order terms’’ of order  $O(f^3)$  with two and more excitations.  $E_{ZP} = -\frac{\Delta_r}{2} + \sum_k \tilde{f}_k (\omega_k \tilde{f}_k - 2c_k)$  is the constant term in  $H_P$ .

Thus, in the polaron picture,  $H_P$  conserves the number of excitations and becomes tractable with the same techniques as RWA models; in particular we can compute the single-excitation eigenstates. It is interesting to note that the GS obtained from the variational method is an eigenstate of  $H_P$  with eigenvalue equal to the GS energy. This gives us a sense of consistency that confirms that the effective RWA model is accurate: If the GS is well caught, one expects that the first excitations are single-particle (quasiparticles) excitations over it.

In Appendix A 6 we show that Eq. (21) admits a bound state below the band, with energy  $E_1$ , and that its localization length is given by

$$\kappa_{\text{SEBS}}^{-1} = \max(\kappa_{\text{GS}}^{-1}, \kappa^{-1}), \quad (22)$$

with  $\kappa \cong \text{arccosh}(\frac{\omega_0 - E_1}{2\lambda})$ . See Appendix A 7 for the proof [cf. Eq. (20)]. In Fig. 4(b) we observe the exponential tails. We observe that, as the qubit bare-frequency increases, the peaks shorten and widen. This is explained by the fact that the total number of excitations is one. Note, however, that the area below the peaks need not be constant, as a varying portion of this excitation is stored in the qubit (it is expected to decrease as  $\Delta$  increases); this phenomenon is shown for the GS in Fig. 2(b) and is also present for the SEBS. Figure 4(c) shows the deexcitation energy for several values of  $\Delta$ , referred to the lower band limit, which means that there exists a bound state below the band for all values of  $\Delta$ .

We can now compare the difference between the results provided by the polaron transform to those obtained using the RWA. Figure 4(a) shows the relative energy difference between the SEBS calculated with each method. The difference increases with  $g$ , becoming significant for  $g \approx 0.1$ . We have shown only one value of  $\Delta$  for clarity, because all

values behaved similarly, with the difference being greater for smaller values of  $\Delta$ . The fact that the PT predicts different bound-state energies is not sufficient to declare it superior to the RWA, it could be the case that these results are worse than those provided by the RWA. The definitive confirmation comes from Fig. 5, where we compare the bosonic spatial distributions from the PT and the RWA with those generated by exact diagonalization of the Hamiltonian for different coupling strengths (see Appendix A 5 for details on the calculation). The results from the PT are in agreement with the numerical results, both in the ground and excited states. In addition, we see how the RWA and PT coincide for low values of  $g$ , but the RWA immediately begins to underestimate the number of photons when the value of  $g$  increases beyond  $g = 0.1$ . Exact diagonalization is limited because the state-space grows exponentially with the number of elements. The use of a Lanczos routine allows us to stretch the capabilities of standard computers, but we still find ourselves limited to a moderate number of sites. In addition, *exact* might be an overstatement considering that one must limit the number of excitations per site in order to have a finite-size Hamiltonian. That is why 22 sites were used in the benchmark for  $g = 0.05$ , a number that had to be reduced for greater values of  $g$  in order to accommodate more excitations per site while maintaining the state-space size allowed by our numerical capabilities (See Fig. 5 for full details).

Finally, let us show that the bound state above the single-photon band that exists in the RWA ( $|E_1^n\rangle$ ) [47,48,81,82], *does not* exist in general in the full model (2). The reason is that this state may be embedded with a continuum of states but with different excitation number. When you add counter-rotating coupling, these states mix and the bound state becomes a Fano resonance. A more detailed explanation is as follows: There is numerical evidence that model (2) has, at least, an even bound state  $|E_2\rangle$  [32]. One can define a band of one-photon states over  $|E_2\rangle$ :  $|k, E_2\rangle$  [83]. The parity of these states is odd. The hypothetical bound state  $|E_1^n\rangle$  would also be odd, since it has one excitation in the RWA limit. This implies that, in order for this state to exist, it cannot be embedded in the band formed by  $|k, E_2\rangle$ , since otherwise they would hybridize. A necessary condition is

$$\omega_0 \geq 4\lambda. \quad (23)$$

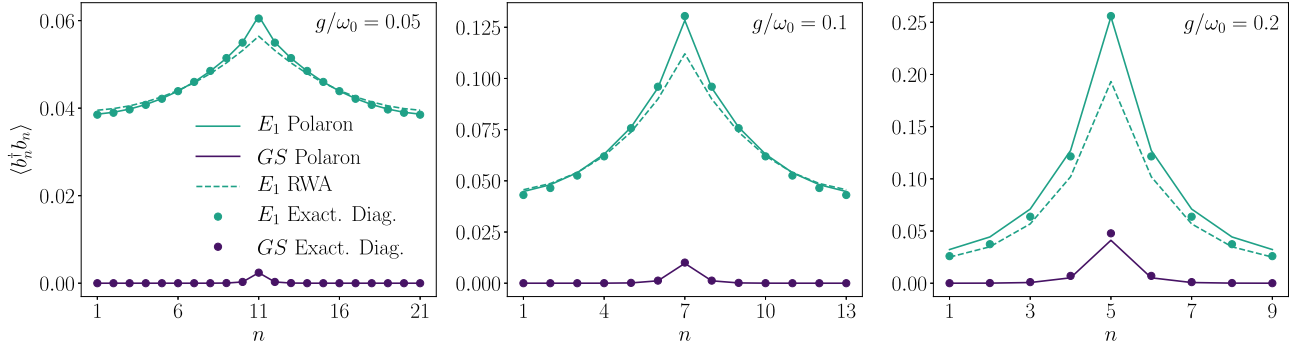


FIG. 5. Comparison of spatial boson distributions from the PT, the RWA, and exact diagonalization. They correspond to  $\Delta = 0.3$ , and  $g = 0.05$ ,  $g = 0.1$ , and  $g = 0.2$ , respectively, from left to right. Solid lines are used to indicate polaron results, dashed lines for RWA results, and dots for exact diagonalization results. A Lanczos routine was used to perform the exact diagonalization: The number of excitations was truncated to 2, 3, and 4 and we used a Lanczos basis size of 150, 200, and 200 for  $g = 0.05$ ,  $g = 0.1$ , and  $g = 0.2$ , respectively, from left to right.

Otherwise,  $|E_1^u\rangle$  does not exist. To demonstrate the latter, we note that the bound-state energy is such that  $E_1^u - E_{GS} > \omega_0 + 2\lambda$ . On the other hand,  $E_2 - E_{GS} < 2(\omega_0 - 2\lambda)$  (i.e., the two-photon band). The overlap occurs (and thus the nonexistence) if  $E_2 + \omega_0 - 2\lambda < E_1^u$ . Putting it all together we arrive at the condition for existence given by Eq. (23). It seems a paradox, since this state does exist in the RWA for all  $\omega_0$  and  $\lambda$ . The puzzle is solved by noting that, in the full model, this state becomes a resonance with a lifetime that diverges in the RWA limit.

### C. Spontaneous emission

To end our analysis of the single-qubit model we discuss the behavior of the system during spontaneous emission. We assume the atom-waveguide in the GS, then the qubit is driven within a  $\pi$  pulse. After the  $\pi$  pulse, the wave function is given by  $|\Psi(0)\rangle = \sigma^+|GS\rangle$ . Since  $[\sigma_x, U_P] = 0$ , we may work in the single-excitation manifold in the polaron picture. Employing the single-excitation Ansatz  $|\psi\rangle_P = (\beta_0\sigma^+ + \sum_k \tilde{\beta}_k a_k^\dagger)|0; \mathbf{0}\rangle$ , the solution is obtained as the inverse Laplace transform  $\beta_0(t) = \mathcal{L}^{-1}[\beta_0(s)]$ , with

$$(s + i\Delta_r)\beta_0(s) = 1 - \sum_k \frac{|\langle 0; \mathbf{0} | a_k H_P \sigma^+ | 0; \mathbf{0} \rangle|^2}{s + i\langle 0; \mathbf{0} | a_k H_P a_k^\dagger | 0; \mathbf{0} \rangle} \beta_0(s). \quad (24)$$

The properties of the (inverse) Laplace transform determine the spontaneous emission. In particular, since  $\langle 0; \mathbf{0} | a_k H_P \sigma^+ | 0; \mathbf{0} \rangle|^2 = 2\Delta_r^2 \tilde{f}_k^2$ , in the continuum limit, the sum in Eq. (24) can be converted to an integral over the spectral density  $J(\omega)$ . Let us discuss the two main contributions to this integral. Far from the band limits,  $J(\omega)$  is sufficiently smooth and the main contribution comes from the poles in the sum, yielding the exponential decay  $\exp[-J(\Delta_r)t]$ . Notice that this is analogous to the RWA result [where the spontaneous emission is  $J(\Delta)$ ] but now it is renormalized [72]. The qualitative difference with the RWA case is the long-time dynamics of  $\beta_0(t)$ , which accounts for the qubit thermalization process. The final value theorem,  $\lim_{s \rightarrow 0} s\beta_0(s) = \lim_{t \rightarrow \infty} \beta_0(t)$ , tells that  $\beta_0 \neq 0$  if some divergence occurs in that integral. This occurs if bound states exist. Physically, this

means that the initially excited state overlaps with the bound state [42,44,64]. This is conveniently calculated by choosing as a basis in the single-excitation manifold

$$\{|E_1\rangle, |E_1\rangle_p^\perp\}, \quad (25)$$

where  $|E_1\rangle$  is the bound state and  $|E_1\rangle_p^\perp$  are all other eigenstates orthogonal to it. We recall that the bound state can be written in terms of the original states spanning the one-excitation subspace

$$|E_1\rangle = \beta_0 |1\rangle |0\rangle + \sum_k \tilde{\beta}_k |0\rangle |1_k\rangle. \quad (26)$$

The first term corresponds to the initial state of the system  $|\psi_0\rangle = |1\rangle |0\rangle$ , which indicates that the initial state has some projection onto the bound state,

$$|\psi_0\rangle = \beta_0 |E_1\rangle + \sum_p \tilde{\beta}_p |E_1\rangle_p^\perp. \quad (27)$$

The projection onto the orthogonal basis states belong to the continuum (scattering states [64]) and, as such, it will not contribute the long-time dynamics. The projection onto the bound state is responsible for the divergence and thus for the nonzero value for  $\beta_0(t \rightarrow \infty)$ . Doing the algebra and computing the observable (notice our return to the laboratory frame) we obtain that

$$\langle \sigma^z(t \rightarrow \infty) \rangle = \beta_0^2 \langle E_1 | U_P^\dagger \sigma^z U_P | E_1 \rangle - (1 - \beta_0^2) \frac{\Delta_r}{\Delta}. \quad (28)$$

In Fig. 6 we confirm this expression. The evolution converges to the stationary value predicted by Eq. (28). Also shown in Fig. 6 is the difference with  $\langle \sigma^z \rangle_{GS} = -\Delta_r/\Delta$ , which becomes significant as the ratio  $g/\Delta$  increases; that is, as the system progresses into the USC regime. Let us emphasize that the last term quantifies the difference to the RWA case, apart from the aforementioned decay renormalization. Another difference is the fact that, in the RWA, some oscillations survive. These arise from the existence of the bound state above the band; without the RWA this bound state becomes instead a resonance, see Sec. III B. In summary, the spontaneous emission example serves to showcase the consequences of USC, in particular the role of qubit renormalization both in

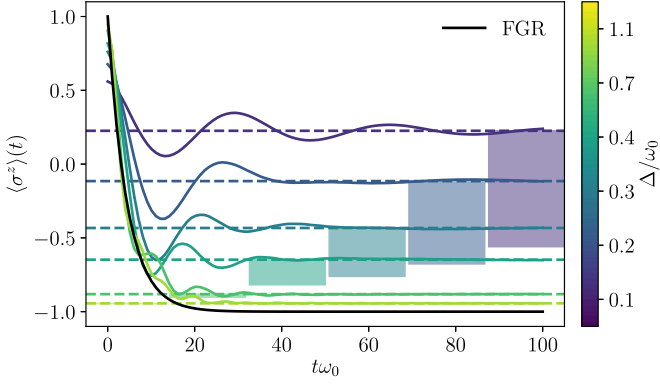


FIG. 6. Evolution of  $\langle \sigma^z \rangle$  (magnetization) for an initially excited qubit as a function of  $\Delta$  for a fixed  $g = 0.3$ . Solid colored lines represent the simulated evolution while dashed colored lines mark the stationary value predicted analytically, Eq. (28). For contrast, the solid black line corresponds to a Markovian evolution, which occurs in the RWA, calculated by applying the Fermi golden rule (FGR) to the excited and ground states for  $\Delta = 1.1$ . Colored shaded boxes have been used to showcase the difference between the stationary magnetization for each  $\Delta$  and the corresponding ground-state magnetization,  $\langle \sigma^z \rangle_{GS}$ .

the equilibrium and out-of-equilibrium dynamics. Finally, it also illustrates the peculiarities of the thermalization process when both the light-matter coupling is nonperturbative and there exist excited bound states.

#### IV. TWO-QUBIT CASE

We now tackle the case of two qubits coupled to the cavity array. Much like in the single-qubit case, we first report the results for the ground state continuing with the bound-state properties. We emphasize the qubit-qubit interactions mediated by the cavity array. As an application, we devise a simple state transfer between two distant qubits that uses those interactions.

##### A. Ground state

Setting  $N_q = 2$  and  $x = x_1 - x_2$  in Eqs. (12) and (13) yields (see Appendixes B 1–B 3) a spin model,

$$\mathcal{H}_S = \frac{\Delta_r}{2} (\sigma_1^z + \sigma_2^z) - \mathcal{J} \sigma_1^x \sigma_2^x + 2 \sum_k \tilde{f}_k (\omega_k \tilde{f}_k - 2c_k), \quad (29)$$

with  $\mathcal{J} = 2 \sum_k \tilde{f}_k (2c_k - \omega_k \tilde{f}_k) \cos(kx)$ , which can be diagonalized to yield a ferromagnetic GS of the form

$$|\text{GS}\rangle_S = \cos \theta |00\rangle + \sin \theta |11\rangle, \quad (30)$$

where  $|00\rangle \equiv |s_1 = 0, s_2 = 0\rangle$  and the coefficients are

$$\cos \theta = \frac{\Delta_r + \sqrt{\Delta_r^2 + \mathcal{J}^2}}{\sqrt{(\Delta_r + \sqrt{\Delta_r^2 + \mathcal{J}^2})^2 + \mathcal{J}^2}}, \quad (31)$$

$$\sin \theta = \frac{\mathcal{J}}{\sqrt{(\Delta_r + \sqrt{\Delta_r^2 + \mathcal{J}^2})^2 + \mathcal{J}^2}}. \quad (32)$$

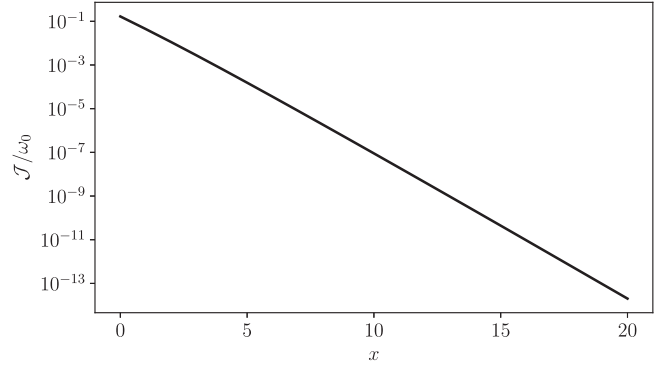


FIG. 7. Dependence of the Ising constant  $\mathcal{J}$  with the distance between the qubits,  $x$ . The behavior is analogous for all values of  $g$ .

By Eq. (11), the GS mean energy is

$$\bar{E}_{GS} = -\sqrt{\Delta_r^2 + \mathcal{J}^2} + 2 \sum_k \tilde{f}_k (\omega_k \tilde{f}_k - 2c_k), \quad (33)$$

which is a minimum for (see Refs. [75,76] and Appendix B 4 for a detailed derivation)

$$\tilde{f}_k = c_k \frac{\mathcal{E} + \mathcal{J} \cos(kx)}{\omega_k \mathcal{E} + \omega_k \mathcal{J} \cos(kx) + \Delta_r^2}. \quad (34)$$

We have introduced the constant  $\mathcal{E} = (\Delta_r^2 + \mathcal{J}^2)^{1/2}$  to ease the notation. It is immediate to check that, should the interaction constant  $\mathcal{J}$  vanish, we would recuperate the expression of  $\tilde{f}_k$  that we found in the single-qubit case. This indeed happens when we set the qubits infinitely far apart, as will be shown shortly. It is also evident that  $\tilde{f}_k$  is even with respect to  $k$ , which matches the restriction we imposed so that the PT could be factored; see Eq. (10). Figure 7 shows that the dependence of  $\mathcal{J}$  on  $x$  is exponential. This implies that the GS is a ferromagnetic state in a short-range Ising model. As such, in a multiqubit scenario, only the interaction with first-nearest neighbors would have to be taken into account. Following our analysis of the single-qubit case, it is useful to study the renormalization of the bare frequency  $\Delta$  with  $g$ . We have used a distance of  $n = 2$  sites to illustrate the deviation from the results obtained in the one-qubit scenario. Figure 8 shows that the influence of the neighboring qubit sharpens the renormalization process, making the system go into full renormalization at lower values of  $g$ . Granted, this effect vanishes if one places the qubits further apart. Due to the exponential decay of  $\mathcal{J}$ , we have found that, at distances of around 20 sites, the results obtained for one and two qubits are indistinguishable.

Back when we studied the single-qubit system, we showed that the probability of having an *excited* spin state was an observable directly related to the renormalization of the bare frequency. The extension to two qubits is straightforward:

$$P_e = \frac{2 + \langle \text{GS} | \sigma_1^z + \sigma_2^z | \text{GS} \rangle_S}{2} = 1 - \frac{\Delta_r}{\Delta} (\cos^2 \theta - \sin^2 \theta), \quad (35)$$

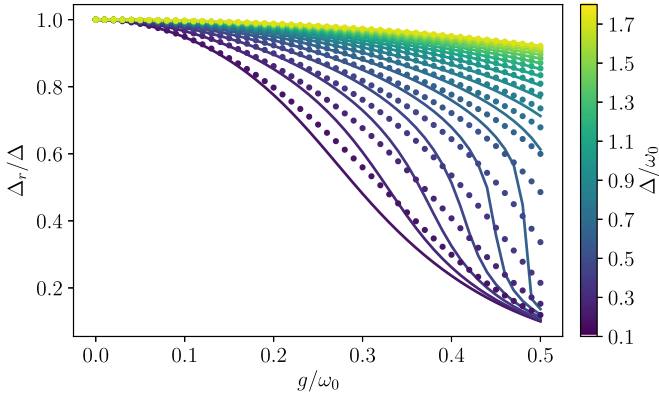


FIG. 8. Renormalization of the bare frequency for  $x = 2$  as a function of  $g$  and  $\Delta$ . Solid lines represent two-qubit results. Dots represent single-qubit results.

where  $|\text{GS}\rangle_S = \cos\theta |00\rangle + \sin\theta |11\rangle$  now. Notice that, at large distances, as  $\mathcal{J} \rightarrow 0$  then  $\cos\theta \rightarrow 1$  and  $\sin\theta \rightarrow 0$ , so Eq. (35) reduces to twice the probability found for a single qubit [Eq. (18)]. The effect of the Ising interaction is revealed at short distances where  $P_e$  deviates from the single-qubit result, no longer equating to the sum of two noninteracting spins. We can again probe the spatial localization of the bosonic cloud. Following the scheme presented in the single-qubit case, we obtain

$$\langle b_n^\dagger b_n \rangle = |f_{n,1}|^2 + |f_{n,2}|^2 + 2 \cos\theta \sin\theta \text{Re} f_{n,1}^* f_{n,2}, \quad (36)$$

where

$$f_{n,j} = \frac{1}{\sqrt{N}} \sum_k e^{ikx_j} \tilde{f}_k e^{-ik(n-N/2)}. \quad (37)$$

See Appendix B 5 for details of this calculation. It is interesting to see the overlap between the two bosonic clouds surrounding each qubit. Figure 9 shows this phenomenon for a value of  $n = 3$  where the overlap is significant. In the same figure, the inset monitors the effect of the coalescence of the clouds as the two qubits approach each other.

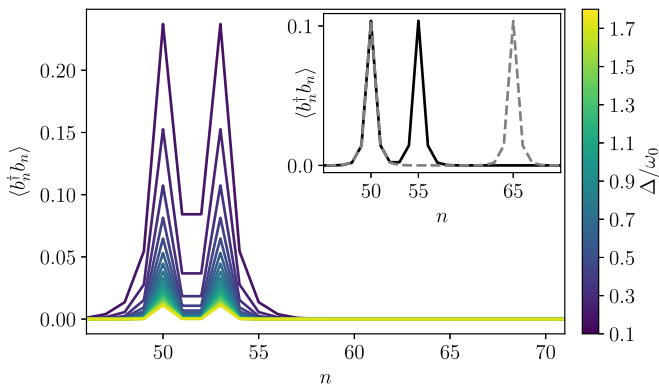


FIG. 9. Spatial distribution of GS of the photons for  $g = 0.3$  and  $x = 3$  as a function of  $\Delta$ , with inset showing the difference in photon-cloud localization when the qubits are placed at distances  $x = 5$  and  $x = 15$  for  $g = 0.3$  and  $\Delta = 0.3$ .

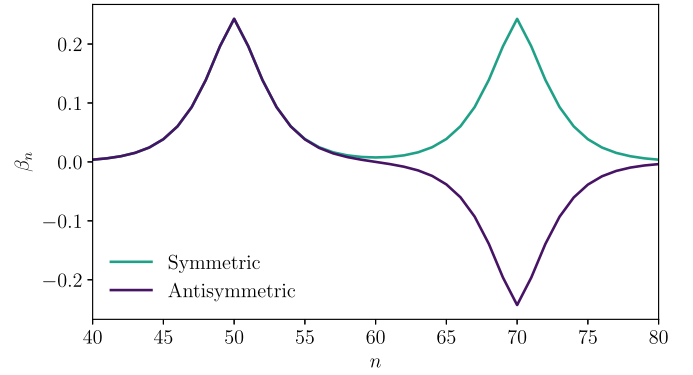


FIG. 10. Symmetric and antisymmetric bound-state wave functions for  $g = 0.3$ ,  $\Delta = 0.3$ , and  $x = 20$ .

## B. Bound states

Analogously to the single-qubit case, we seek an effective Hamiltonian for the two-qubit model that is a good approximation of the full Hamiltonian but conserves the number of excitations, allowing us to restrict our search for bound states to the one-excitation subspace. We have discussed how  $\tilde{f}_k$  for two-qubits converges to the expression of  $\tilde{f}_k$  for a single qubit, so if we assume  $\mathcal{J}$  to be small, we can write

$$\tilde{f}_k = \tilde{f}_k^0 + \delta(\tilde{f}_k), \quad (38)$$

where  $\tilde{f}_k^0$  is the single-qubit  $\tilde{f}_k$  defined in Eq. (16) and  $\delta(\tilde{f}_k)$  encapsulates the remainder of the two-qubit  $\tilde{f}_k$ . This allows us to reach the effective Hamiltonian

$$\begin{aligned} H_P = & \frac{\Delta_r}{2} (\sigma_1^z + \sigma_2^z) - 2\Delta_r \sum_j \sigma_j^z \sum_{k,p} \tilde{f}_k \tilde{f}_p e^{i(k-p)x_j} b_k^\dagger b_p \\ & + \sum_{j,k} [2\Delta_r \tilde{f}_k^0 + \delta(\tilde{f}_k)(\Delta_r - \omega_k)] (\sigma_j^- b_k^\dagger e^{ikx_j} + \text{H.c.}) \\ & + \sum_k \omega_k b_k^\dagger b_k - \mathcal{J} \sigma_1^x \sigma_2^x + E_{ZP}. \end{aligned} \quad (39)$$

Above, we discarded terms such as  $\delta(\tilde{f}_k) \sigma_j^+ b_k^\dagger$  owing to the fact that  $\delta(\tilde{f}_k)$  is small for small  $\mathcal{J}$ . This must be compared with the single-qubit case, where the number-conserving, effective, single-particle Hamiltonian arose naturally [cf. Eq. (21)].

Once again, we can diagonalize the restriction of  $H_P$  in search of states whose energy lies below the band limit and are, thus, bound. In this case, we expect to find two bound states, corresponding to the symmetric and antisymmetric combination of the wave functions corresponding to each single-qubit bound state (see Fig. 10). A general eigenstate of  $H_P$  has the form

$$|\psi\rangle_P = \left( \beta_1 \sigma_1^+ + \beta_2 \sigma_2^+ + \sum_k \tilde{\beta}_k a_k^\dagger \right) |\text{GS}\rangle. \quad (40)$$

The reader might recall that, in the single-qubit case, the one-excitation subspace was spanned by  $|1\rangle|0\rangle$  and  $|0\rangle|1_k\rangle$  and wonder why we cannot substitute  $|S\rangle|1_k\rangle$  by  $|00\rangle|1_k\rangle$  in the two-qubit basis. In that sense, it must be

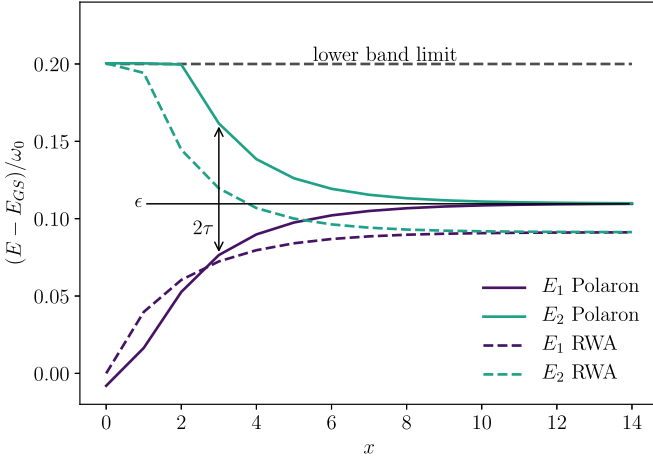


FIG. 11. Energy difference between symmetric and antisymmetric bound states as a function of  $x$ , the distance between qubits for  $g = 0.3$  and  $\Delta = 0.3$  (a value of  $x = 0$  indicates that the two qubits are coupled to the same cavity). Dashed lines represent RWA results and solid lines represent polaron results.

clarified that we seek to work in a subspace that is one excitation above the GS, regardless of however many excitations the GS contains. The proposed state, Eq. (40), on the other hand, comes with a problem since the subspace spanned by Eq. (40) is not closed under the action of the Hamiltonian, e.g.,  $\sigma_1^- a_k^\dagger |10\rangle |0_k\rangle = \cos(\theta) |GS\rangle_S |1_k\rangle + \sin(\theta) (-\sin(\theta) |00\rangle + \cos(\theta) |11\rangle) |1_k\rangle$ . Fortunately, this second contribution is of second order in  $\tilde{f}_k$ . Besides, the terms containing  $\sigma_1^- a_k^\dagger$  in Hamiltonian (39) are of the order of  $\tilde{f}_k$ . Thus they are h.o.t. that, consistent with Eq. (21), are discarded.

Figure 10 shows  $\beta_n$  for the two lowest-energy eigenstates, where  $\beta_n$  is obtained by Fourier transforming  $\beta_k$  in Eq. (40). In the single-qubit case, we showed that there exists a bound state in the form of a cloud of virtual photons localized around the qubit. We have also shown that two sufficiently distant qubits do not interact and, as such, their wave functions do not overlap, contributing two bound states of equal energy to the spectrum. As the two qubits approach, we expect the increasing overlap to break the degeneracy and split the two bound states into different energies. If that is the case, the interaction can cause the energy of the antisymmetric state to rise above the lower band limit, forcing it to no longer be bound (nor antisymmetric), because the corresponding photons have an allowed frequency in the waveguide, and as such they no longer exhibit exponential decay. These oscillating eigenstates are referred to as scattering states [64]. Figure 11 shows the aforementioned effect. In the figure we also compare our results with those obtained within the RWA. We conclude that the latter underestimates the interaction between the two bound states (see below). In Fig. 12 a comparison between the spatial distribution of photons for two different distances is drawn. As the two qubits approach, the difference in profiles becomes significant and, should they reach  $n = 2$ , the antisymmetric bound state would cease to exist as it enters the allowed frequency band. See Appendix B 6 for a calculation of  $\langle b_n^\dagger b_n \rangle$ .

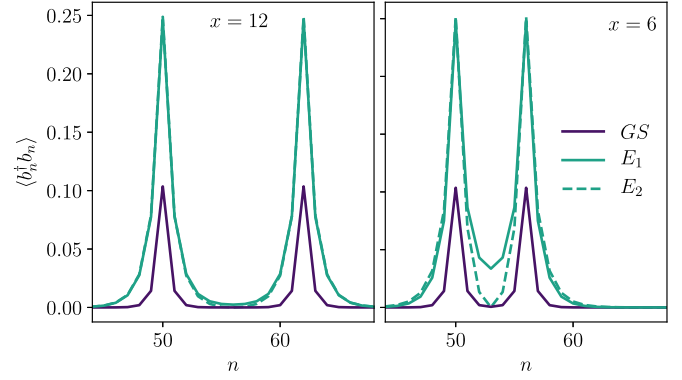


FIG. 12. Comparison of spatial photon distributions of the symmetric ( $E_1$ ) and antisymmetric ( $E_2$ ) bound states for  $g = 0.3$  and  $\Delta = 0.3$  at two different distances:  $x = 12$  and  $x = 6$ .

### C. State transfer

Inspired by Fig. 11 and restricting ourselves to the two bound states we can define a tight-binding Hamiltonian

$$H_{TB} = \sum_{i=L,R} \epsilon |i\rangle \langle i| + \sum_{\substack{i,j=L,R \\ i \neq j}} \tau |i\rangle \langle j|, \quad (41)$$

where  $|L\rangle$  represents the bound state of the left-most qubit and  $|R\rangle$  represents the bound state of the right-most qubit. The eigenstates of  $H_{TB}$  are the symmetric and antisymmetric combinations of  $|L\rangle$  and  $|R\rangle$ , provided  $\tau \neq 0$ , with respective energies  $\epsilon - \tau$  and  $\epsilon + \tau$ . This simplified model is the basis for the study of effective interactions between bound states, which, as we introduced, provides a means to engineer lossless state transfer protocols through virtual photons, one of the main objectives of our work. Real, propagating photons can be used to transport information between distant qubits but, even in one-dimensional arrays where an emitted photon travels nondissipatively, there exist undesired losses intrinsic to the emission process. The reason is simple, in the absence of anisotropies, it is equally likely that a radiated photon will travel in the direction of the neighboring qubit as it is for it to travel in the opposite direction, and thus be lost. The transmission of information via virtual photons bypasses this limitation. By virtue of them being nonradiative, there is no loss; information is shared between close qubits through the overlap of their photonic clouds.

To exemplify perfect lossless state transfer using bound states, we propose the protocol shown in Fig. 13. Its purpose is to transfer the excited state from one qubit to the other deterministically. We assume that  $g_1$  and  $g_2$ , the coupling constant of each qubit to the waveguide, can be tuned independently. First, the left-most qubit is initialized in its excited state and the other is kept in its ground state while both are uncoupled from the waveguide. We set  $\Delta < \omega_0 - 2\lambda$ , i.e., this state lies outside the band. In addition it has odd parity; in fact, it is the minimum-energy state with odd parity. At  $t_0$ ,  $g_1$  is increased adiabatically, so that this state becomes a bound state. Arguing within the Adiabatic Theorem, it will remain a bound state by doing the adiabatic ramp slow enough. It is worth recalling

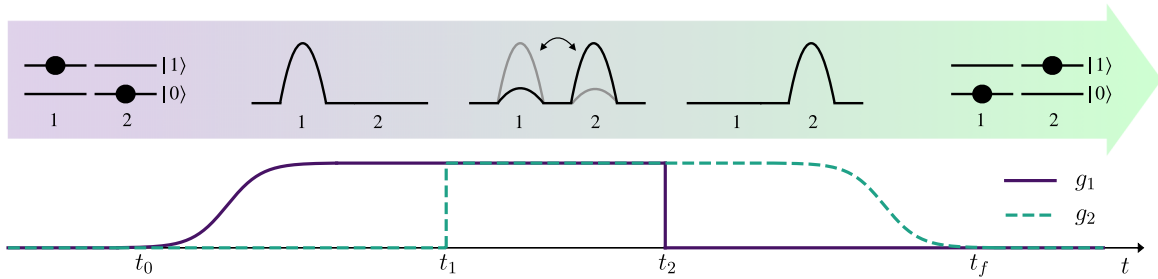


FIG. 13. State transfer protocol between two qubits coupled to the same linear cavity array with distinct tunable coupling constants  $g_1$  and  $g_2$ . Bound states are depicted as parabolic instead of exponential for aesthetic purposes.

that here, possible nonadiabatic transitions are avoidable since the bound state separates from the band (odd states) as  $g$  increases. So, the minimum gap is  $\omega_0 - 2\lambda - \Delta$  that can be adjusted *a priori*. Then, at  $t_1$ ,  $g_2$  is increased diabatically to match  $g_1$ . This sudden change in the Hamiltonian does not allow the state to evolve quasistatically into the new eigenstate and instead gives rise to Rabi oscillations between the left and right bound states, whose symmetric and antisymmetric combinations are actually the eigenstates of the new Hamiltonian. Knowing the hopping frequency  $\tau$ , we can interrupt the dynamics, by diabatically zeroing  $g_1$  at  $t_2$ , at the precise moment where the system is fully in the right bound state, i.e.,  $t_2 - t_1 = \pi/4\tau$ , see Eq. (41). Finally,  $g_2$  is lowered adiabatically, so the right bound state transforms into an excited right-most qubit, successfully completing the state-transfer protocol at  $t_f$ . This protocol can be applied sequentially to a succession of qubits to effectively transport a state along the waveguide.

It is important to note that this method is limited by the fact that the interaction decays exponentially, and this limitation is twofold. First, an exponential decay means that, in order to transport a state between distant qubits, many ancilla qubits are required, placed in close formation, so that there exists an effective interaction among every pair of consecutive qubits. For every qubit added to the chain, the system becomes more susceptible to decoherence and losses. In addition, the hopping frequency  $\tau$ , which is proportional to the coupling, is what determines the speed at which a single iteration of the protocol can be performed, so it is against our interest that the coupling decays so rapidly. One may even doubt if an exponentially decaying effective interaction would be, at any range, intense enough to not be overpowered by spurious dipole-dipole interactions between the qubits, which decay more slowly, with a power law. Fortunately, we can assure that the effective interaction is orders of magnitude greater than dipole-dipole interactions, since the latter is of the order of  $10^{-4}$  eV for nearest neighbors within a crystal lattice ( $d \approx 1$  Å).<sup>2</sup> In our setup, there is a non-negligible interaction up to distances of around 3 sites, which in

experimental realizations of quantum circuits have sizes of millimeters.

## V. CONCLUSIONS

We have discussed the main properties of bound states in waveguide QED beyond the RWA paradigm. In other words, we have quantified the corrections to the *standard* calculations where the qubit-photon interaction is assumed to be number conserving based on the perturbative character of the latter. We have shown that the polaron technique is useful. It provides a unitary transformation that disentangles qubits and waveguide and the interaction, within this picture, is effectively number conserving. Therefore, it allows us to export techniques such as the Weisskopf-Wigner theory and intuitions to a broader range of light-matter coupling strengths where the RWA fails.

The main results discussed in the paper are as follows: We have extended the calculations for the spontaneous emission up to moderate light-matter couplings obtaining a renormalization of the rate (due to the qubit-frequency renormalization). The existence criterion for bound states has been generalized and its role in the thermalization of the qubits has been discussed. Finally, we have computed the effective spin-spin interactions both through vacuum fluctuations and bound states. We sketched a perfect state transfer protocol among bound states.

## ACKNOWLEDGMENTS

This work has been supported by the EU (COST Action 15128 MolSpin on Molecular Spintronics, QUANTERA SUMO project and the Spanish MICINN Grant No. MAT2017-88358-C3-1-R. J.R.-R. is supported by ICMA through a PI2-ICMA contract. Eduardo Sánchez-Burillo acknowledges an ERC Advanced Grant QUENOCOBA under the EU Horizon 2020 program (Grant Agreement No. 742102).

## APPENDIX A: SINGLE QUBIT: SOME DETAILS OF THE CALCULATIONS

### 1. Derivation of the basic commutation relations

We will use the following property: Let  $A$ ,  $B$ , and  $C$  be operators such that  $[B, A] = C$  and  $[C, A] = 0$ , then  $[B, e^A] = Ce^A$  also holds. The proof is by induction.

<sup>2</sup>To exemplify the weakness of the dipole-dipole interaction, it is insightful to remember that it was not strong enough to explain ferromagnetism in solids. The *exchange interaction* had to be introduced in the study of ferromagnetism for this very reason.

Using this property, we arrive at the basic commutation relations.

$$\begin{aligned} [b_k, A] &= -\sigma^x (\tilde{f}_k [b_k, b_k^\dagger] - \tilde{f}_k [b_k, b_k]) \\ &= -\tilde{f}_k \sigma^x \rightarrow [b_k, U_P] = -\tilde{f}_k \sigma^x U_P, \end{aligned} \quad (\text{A1})$$

$$\begin{aligned} [b_k^\dagger, A] &= -\sigma^x (\tilde{f}_k [b_k^\dagger, b_k^\dagger] - \tilde{f}_k [b_k^\dagger, b_k]) \\ &= -\tilde{f}_k \sigma^x \rightarrow [b_k^\dagger, U_P] = -\tilde{f}_k \sigma^x U_P. \end{aligned} \quad (\text{A2})$$

## 2. Calculation of $\langle b_n^\dagger b_n \rangle$ for the ground state of a single qubit

$$\begin{aligned} \langle b_n^\dagger b_n \rangle &= \langle \text{GS} | b_n^\dagger b_n | \text{GS} \rangle \\ &= \langle \text{GS} | \frac{1}{\sqrt{N}} \sum_k e^{ik(n-N/2)} b_k^\dagger \frac{1}{\sqrt{N}} \sum_p e^{-ip(n-N/2)} b_p | \text{GS} \rangle \\ &= \frac{1}{N} \sum_{k,p} e^{i(k-p)(n-N/2)} \langle 00 | U_P^\dagger b_k^\dagger b_p U_P | 00 \rangle. \end{aligned} \quad (\text{A3})$$

To continue, we must first calculate  $U_P^\dagger b_k^\dagger b_p U_P$ . Since we have already taken  $\tilde{f}_k$  as real in previous calculations, we assume it to be real here as well:

$$\begin{aligned} U_P^\dagger b_k^\dagger b_p U_P &= U_P^\dagger (b_k^\dagger [b_p, U_P] + [b_k^\dagger, U_P] b_p) + b_k^\dagger b_p \\ &= U_P^\dagger (-\tilde{f}_p \sigma^x b_k^\dagger U_P - \tilde{f}_k \sigma^x U_P b_p) + b_k^\dagger b_p \\ &= U_P^\dagger (-\tilde{f}_p \sigma^x [b_k^\dagger, U_P] - \tilde{f}_p \sigma^x U_P b_k^\dagger - \tilde{f}_k \sigma^x U_P b_p) + b_k^\dagger b_p \\ &= U_P^\dagger (U_P \tilde{f}_k \tilde{f}_p - \tilde{f}_p \sigma^x U_P b_k^\dagger - \tilde{f}_k \sigma^x U_P b_p) + b_k^\dagger b_p \\ &= \tilde{f}_k \tilde{f}_p - \sigma^x (\tilde{f}_p b_k^\dagger + \tilde{f}_k b_p) + b_k^\dagger b_p. \end{aligned} \quad (\text{A4})$$

We are now equipped with the necessary ingredients to compute  $\langle 00 | U_P^\dagger b_k^\dagger b_p U_P | 00 \rangle$ . Considering that the state  $|00\rangle$  does not connect through the second and third terms, the mean value is just  $\tilde{f}_k \tilde{f}_p$ .

With that, we simply have

$$\begin{aligned} \langle = | b_n^\dagger b_n | = \rangle &= \frac{1}{\sqrt{N}} \sum_k e^{ik(n-N/2)} \tilde{f}_k \frac{1}{\sqrt{N}} \sum_p e^{-ip(n-N/2)} \tilde{f}_p \\ &= f_n^* f_n = f_n^2. \end{aligned} \quad (\text{A5})$$

## 3. Exponential localization of the ground state

We recall that

$$\tilde{f}_k = \frac{g}{\sqrt{N}(\Delta_r + \omega_k)}, \quad (\text{A6})$$

with

$$\omega_k = \omega_0 - 2\lambda \cos k. \quad (\text{A7})$$

Noticing that

$$\mathcal{F}[e^{-\kappa_{\text{GS}}|n-N/2|}] = \frac{1}{\sqrt{N}} \frac{1 - e^{-2\kappa_{\text{GS}}}}{1 + e^{-2\kappa_{\text{GS}}} + 2e^{-\kappa_{\text{GS}}} \cos k}, \quad (\text{A8})$$

with *our* convention for the Fourier transform  $\mathcal{F}[g(n)] = \sum_0^{N-1} e^{ik(n-N/2)} g(n)$ , yields Eq. (20) in the main text.

## 4. Single qubit effective Hamiltonian

The strict application of the polaron transform to the original Hamiltonian,  $H_P = U_P^\dagger H U_P$ , yields the transformed Hamiltonian

$$\begin{aligned} H_P &= \frac{\Delta}{2} \exp \left[ 2\sigma^x \sum_k \tilde{f}_k b_k^\dagger - \tilde{f}_k b_k \right] \sigma^z + \sum_k \omega_k b_k^\dagger b_k + \Delta_r \sigma^x \\ &\times \sum_k \tilde{f}_k (b_k^\dagger + b_k) + E_{\text{ZP}}. \end{aligned} \quad (\text{A9})$$

We can further simplify it by expanding the exponential term. Making use of the Baker-Campbell-Hausdorff formula we get

$$\begin{aligned} &\exp \left[ 2\sigma^x \sum_k \tilde{f}_k b_k^\dagger - \tilde{f}_k b_k \right] \\ &= \exp \left[ -2 \sum_k \tilde{f}_k^2 \right] \exp \left[ 2\sigma^x \sum_k \tilde{f}_k b_k^\dagger \right] \\ &\times \exp \left[ -2\sigma^x \sum_k \tilde{f}_k b_k \right]. \end{aligned} \quad (\text{A10})$$

A power series expansions of the nonconstant terms gives

$$\exp \left[ 2\sigma^x \sum_k \tilde{f}_k b_k^\dagger \right] = 1 + 2\sigma^x \sum_k \tilde{f}_k b_k^\dagger + \dots, \quad (\text{A11})$$

$$\exp \left[ -2\sigma^x \sum_k \tilde{f}_k b_k \right] = 1 - 2\sigma^x \sum_k \tilde{f}_k b_k + \dots. \quad (\text{A12})$$

Ignoring higher-order terms, as well as second-order number-nonconserving terms of the form  $b_k^\dagger b_p^\dagger$  and H.c., the right-hand side of Eq. (A10) becomes

$$\begin{aligned} &\exp \left[ -2 \sum_k \tilde{f}_k^2 \right] \\ &\times \left( 1 + 2\sigma^x \sum_k \tilde{f}_k (b_k^\dagger - b_k) - 4 \sum_{k,p} \tilde{f}_k \tilde{f}_p b_k^\dagger b_p \right). \end{aligned} \quad (\text{A13})$$

Reintroducing this result in  $H_P$  yields

$$\begin{aligned} H_P &= \frac{\Delta_r}{2} \sigma^z + \Delta_r \sigma^x \sigma^z \sum_k \tilde{f}_k (b_k^\dagger - b_k) - 2\Delta_r \sum_{k,p} \tilde{f}_k \tilde{f}_p b_k^\dagger b_p \\ &+ \sum_k \omega_k b_k^\dagger b_k + \Delta_r \sigma^x \sum_k \tilde{f}_k (b_k^\dagger + b_k) + E_{\text{ZP}}. \end{aligned} \quad (\text{A14})$$

Considering that  $\sigma^x \sigma^z + \sigma^x = 2\sigma^-$  and  $-\sigma^x \sigma^z + \sigma^x = 2\sigma^+$  we can combine the second and second-to-last terms to arrive at the final expression for  $H_P$ :

$$\begin{aligned} H_{\text{eff}} &= \frac{\Delta_r}{2} \sigma^z + \sum_k \omega_k b_k^\dagger b_k + 2\Delta_r \sum_k \tilde{f}_k (\sigma^- b_k^\dagger - \sigma^+ b_k) \\ &- 2\Delta_r \sum_{k,p} \tilde{f}_k \tilde{f}_p b_k^\dagger b_p + E_{\text{ZP}}. \end{aligned} \quad (\text{A15})$$

### 5. Calculation of $\langle b_n^\dagger b_n \rangle$ for the single-excitation bound state of a single qubit

The SEBS will be a state of the form

$$|v\rangle = \beta_0 |1\rangle |0\rangle + \sum_k \tilde{\beta}_k |0\rangle |1_k\rangle. \quad (\text{A16})$$

Thus

$$\begin{aligned} \langle b_n^\dagger b_n \rangle &= \langle v | b_n^\dagger b_n | v \rangle \\ &= \langle v | \frac{1}{\sqrt{N}} \sum_k e^{ik(n-N/2)} b_k^\dagger \frac{1}{\sqrt{N}} \sum_p e^{-ip(n-N/2)} b_p | v \rangle \\ &= \frac{1}{N} \sum_{k,p} e^{i(k-p)(n-N/2)} \langle v | U_p^\dagger b_k^\dagger b_p U_p | v \rangle. \end{aligned} \quad (\text{A17})$$

In Appendix A2 we saw that  $U_p^\dagger b_k^\dagger b_p U_p = \tilde{f}_k \tilde{f}_p - \sigma^x (\tilde{f}_p b_k^\dagger + \tilde{f}_k b_p) + b_k^\dagger b_p$ . The first term is constant, so  $|v\rangle$  connects entirely, yielding  $\tilde{f}_k \tilde{f}_p$ . The last term only connects the bosonic part of  $|v\rangle$  to give  $\tilde{\beta}_k \tilde{\beta}_k$ . Finally, the second term cross connects the two components of  $|v\rangle$ , resulting in  $\beta_0 \tilde{f}_p \tilde{\beta}_k^* + \beta_0 \tilde{f}_k \tilde{\beta}_k$ . Reintroducing these partial results into Eq. (A17), one has

$$\begin{aligned} \langle |b_n^\dagger b_n| \rangle &= f_n^2 + \beta_n^2 + \beta_0 f_n^* \beta_n^* + \beta_0 f_n \beta_n = f_n^2 + \beta_n^2 \\ &+ 2\beta_0 \text{Re} f_n \beta_n. \end{aligned} \quad (\text{A18})$$

### 6. Existence of bound states in ultrastrong coupling regime

We work in the polaron picture. A non-normalized single excitation is

$$|\psi_1\rangle_P = \beta_0 |1, 0\rangle + \sum_k \tilde{\beta}_k |0, 1_k\rangle. \quad (\text{A19})$$

It is an eigenstate if and only if

$$\Delta_r - \sum_k \tilde{\beta}_k 2\Delta_r \tilde{f}_k = E, \quad (\text{A20a})$$

$$\tilde{\beta}_k \omega_k - 2\Delta_r \tilde{f}_k + 2\Delta_r \tilde{\beta}_k \sum_{k'} \tilde{f}_k f_{k'} = E \tilde{\beta}_k. \quad (\text{A20b})$$

The solution for  $E$  is found by searching for the zeros of the function  $F(E)$  (cf. with the RWA case in Ref. [47]):

$$F_1(E) = E - \left( \Delta_r + \sum_k \frac{(2\Delta_r \tilde{f}_k)^2}{E - \omega_k - 2\Delta_r \sum_{k'} \tilde{f}_k f_{k'}} \right). \quad (\text{A21})$$

If  $E < \min[\omega_k]$ , the state is a SEBS. Notice that the term in brackets is a monotonically decreasing function with  $g$ . Therefore, if a bound state exists for  $g \rightarrow 0^+$  then it exists for any finite value of  $g$ . For our model in the limit  $g \rightarrow 0^+$  a bound state below the band exists [47], thus the existence of bound states in the USC is guaranteed.

### 7. Localization length

Apart from their existence, the key property of bound states is their localization length. From Eq. (A20b) we obtain

$$\tilde{\beta}_k = \frac{2\Delta_r \tilde{f}_k}{\omega_k - E_1 + 2\Delta_r \sum_{k'} \tilde{f}_k f_{k'}}. \quad (\text{A22})$$

In the low- $g$  regime  $2\Delta_r \tilde{f}_k \approx g$  and we can neglect the term  $2\Delta_r \sum_{k'} \tilde{f}_k f_{k'}$ ; therefore, by simple inspection we see that

$\mathcal{F}^{-1}[\tilde{\beta}_k] = \beta_n \sim e^{-\kappa n}$  with

$$\kappa_1 \cong \text{arccosh}\left(\frac{\omega_0 - E_1}{2\lambda}\right). \quad (\text{A23})$$

Looking at Eq. (A18), Appendix A3, and Eq. (20), the localization is given by  $\kappa_{\text{SEBS}}^{-1} = \max(\kappa_{\text{GS}}^{-1}, \kappa^{-1})$  as given by Eq. (22).

## APPENDIX B: CALCULATIONS FOR THE TWO-QUBIT CASE

### 1. Derivation of the basic commutation relations

Recycling much of the work done in Appendix A1, we simply see that

$$\begin{aligned} [b_k, A_j] &= -\sigma_j^x (\tilde{f}_k e^{ikx_j} [b_k, b_k^\dagger] - \tilde{f}_k e^{-ikx_j} [b_k, b_k]) \\ &= -\sigma^x \tilde{f}_k e^{ikx_j} \rightarrow [b_k, U_j] = -\sigma^x \tilde{f}_k e^{ikx_j} U_j, \end{aligned} \quad (\text{B1})$$

$$\begin{aligned} [b_k^\dagger, A_j] &= -\sigma_j^x (\tilde{f}_k e^{ikx_j} [b_k^\dagger, b_k^\dagger] - \tilde{f}_k e^{-ikx_j} [b_k^\dagger, b_k]) \\ &= -\sigma^x \tilde{f}_k e^{-ikx_j} \rightarrow [b_k^\dagger, U_j] = -\sigma^x \tilde{f}_k e^{-ikx_j} U_j. \end{aligned} \quad (\text{B2})$$

### 2. Calculation of $H_I$

In an attempt to lighten notation we have omitted the summation signs  $\sum$  in the following calculation. They will be reintroduced when we present the final result. It must be understood that there is a summation over all indexes present; for instance,

$$\sigma_j^x c_k (b_k^\dagger e^{ikx_j} + b_k e^{-ikx_j}) \equiv \sum_j \sigma_j^x \sum_k c_k (b_k^\dagger e^{ikx_j} + b_k e^{-ikx_j}). \quad (\text{B3})$$

We thus have

$$U_P^\dagger H_I U_P = U_2^\dagger U_1^\dagger (H_I^1 + H_I^2) U_1 U_2. \quad (\text{B4})$$

We can focus on  $H_I^1$  and the results will be perfectly extensible to  $H_I^2$ .

Hence, making use of the basic commutation relations, [Eqs. (B1), (B2)],

$$\begin{aligned} U_2^\dagger U_1^\dagger H_I^1 U_1 U_2 &= U_2^\dagger U_1^\dagger \sigma_1^x c_k (b_k^\dagger e^{ikx_1} + b_k e^{-ikx_1}) U_1 U_2 \\ &= U_2^\dagger [\sigma_1^x c_k (-\sigma_1^x e^{ikx_1} \tilde{f}_k e^{-ikx_1} - \sigma_1^x e^{-ikx_1} \tilde{f}_k e^{ikx_1}) + H_I^1] U_2 \\ &= U_2^\dagger (-2c_k \tilde{f}_k + H_I^1) U_2 = -2c_k \tilde{f}_k + U_2^\dagger H_I^1 U_2 \\ &= -2c_k \tilde{f}_k + U_2^\dagger [\sigma_1^x c_k (b_k^\dagger e^{ikx_1} + b_k e^{-ikx_1})] U_2 \\ &= -2c_k \tilde{f}_k + \sigma_1^x c_k (-\sigma_2^x e^{ikx_1} \tilde{f}_k e^{-ikx_2} - \sigma_2^x e^{-ikx_1} \tilde{f}_k e^{ikx_2}) + H_I^1 \\ &= -2c_k \tilde{f}_k - 2\sigma_1^x \sigma_2^x c_k \tilde{f}_k \cos(kx) + H_I^1. \end{aligned} \quad (\text{B5})$$

Likewise,

$$U_2^\dagger U_1^\dagger H_I^2 U_1 U_2 = -2c_k \tilde{f}_k - 2\sigma_1^x \sigma_2^x c_k \tilde{f}_k \cos(kx) + H_I^2. \quad (\text{B6})$$

And finally,

$$U_P^\dagger H_I U_P = -4 \sum_k c_k \tilde{f}_k - 4\sigma_1^x \sigma_2^x \sum_k c_k \tilde{f}_k \cos(kx) + H_I. \quad (\text{B7})$$

### 3. Calculation of $H_B$

Much like in Appendix B 2 we have omitted the summation signs for the calculation.

$$\begin{aligned}
 U_P^\dagger H_B U_P &= U_2^\dagger U_1^\dagger \omega_k b_k^\dagger b_k U_1 U_2 \\
 &= \omega_k U_2^\dagger [U_1^\dagger (b_k^\dagger [b_k, U_1] + [b_k^\dagger, U_1] b_k) + H_B/\omega_k] \\
 &= \omega_k U_2^\dagger [U_1^\dagger (-\sigma_1^x b_k^\dagger \tilde{f}_k e^{ikx_1} U_1 - \sigma \tilde{f}_k e^{-ikx_1} U_1 b_k) + H_B/\omega_k] U_2 \\
 &= \omega_k U_2^\dagger \{U_1^\dagger [-\sigma_1^x \tilde{f}_k e^{ikx_1} (U_1 b_k^\dagger - \sigma_1^x \tilde{f}_k e^{-ikx_1} U_1) - \sigma_1^x \tilde{f}_k e^{-ikx_1} U_1 b_k] + H_B/\omega_k\} U_2 \\
 &= \omega_k U_2^\dagger [-\sigma_1^x \tilde{f}_k (b_k^\dagger e^{ikx_1} + b_k e^{-ikx_1}) + \tilde{f}_k^2 + H_B/\omega_k] U_2 \\
 &= H_B + \omega_k \{2\tilde{f}_k^2 - \sigma_1^x \tilde{f}_k (b_k^\dagger e^{ikx_1} + b_k e^{-ikx_1}) - \sigma_2^x \tilde{f}_k (b_k^\dagger e^{ikx_2} + b_k e^{-ikx_2}) + U_2^\dagger [-\sigma_1^x \tilde{f}_k (b_k^\dagger e^{ikx_1} + b_k e^{-ikx_1}), U_2]\} \\
 &= H_B + \omega_k [2\tilde{f}_k^2 - \sigma_j^x \tilde{f}_k (b_k^\dagger e^{ikx_j} + b_k e^{-ikx_j}) - \sigma_1^x \tilde{f}_k (-\sigma_2^x e^{ikx_1} \tilde{f}_k e^{-ikx_2} - \sigma_2^x e^{-ikx_1} \tilde{f}_k e^{ikx_2})] \\
 &= \omega_k \{2\tilde{f}_k^2 - \sigma_j^x \tilde{f}_k (b_k^\dagger e^{ikx_j} + b_k e^{-ikx_j}) + 2\sigma_1^x \sigma_2^x \tilde{f}_k^2 \cos[k(x_2 - x_1)]\} + H_B. \tag{B8}
 \end{aligned}$$

So finally,

$$U_P^\dagger H_B U_P = 2 \sum_k \omega_k \tilde{f}_k^2 + 2\sigma_1^x \sigma_2^x \sum_k \omega_k \tilde{f}_k^2 \cos(kx) - \sum_j \sigma_j^x \sum_k \omega_k \tilde{f}_k (b_k^\dagger e^{ikx_j} + b_k e^{-ikx_j}) + \sum_k \omega_k b_k^\dagger b_k. \tag{B9}$$

### 4. Calculation of the minimal value of $\tilde{f}_k$

The explicit dependence of  $\bar{E}_{GS}$  with  $\tilde{f}_k$  is

$$\begin{aligned}
 \bar{E}_{GS} &= -\mathcal{E} + 2 \sum_k \tilde{f}_k (\omega_k \tilde{f}_k - 2c_k) = -\sqrt{\Delta_r^2 + \mathcal{J}^2} + 2 \sum_k \tilde{f}_k (\omega_k \tilde{f}_k - 2c_k) \\
 &= -\sqrt{4 \left[ \sum_k \tilde{f}_k (2c_k - \omega_k \tilde{f}_k) \cos(kx) \right]^2 + \Delta^2 \exp \left[ -4 \sum_k \tilde{f}_k^2 \right]} + 2 \sum_k \tilde{f}_k (\omega_k \tilde{f}_k - 2c_k). \tag{B10}
 \end{aligned}$$

Thus

$$\frac{\partial \bar{E}_{GS}}{\partial \tilde{f}_k} = -\frac{4\mathcal{J}(2c_k - 2\omega_k \tilde{f}_k) \cos(kx) - 8\tilde{f}_k \Delta_r^2}{2\mathcal{E}} + 2(2\omega_k \tilde{f}_k - 2c_k) = 0 \rightarrow \tilde{f}_k = c_k \frac{\mathcal{E} + \mathcal{J} \cos(kx)}{\mathcal{E} \omega_k + \mathcal{J} \omega_k \cos(kx) + \Delta_r^2}. \tag{B11}$$

### 5. Calculation of $\langle b_n^\dagger b_n \rangle$ for the ground state of two-qubit scenario

The ground state is

$$|\text{GS}\rangle = (\alpha |00\rangle + \beta |11\rangle) |0\rangle. \tag{B12}$$

Thus

$$\langle b_n^\dagger b_n \rangle = \langle \text{GS} | b_n^\dagger b_n | \text{GS} \rangle = \langle \text{GS} | \frac{1}{\sqrt{N}} \sum_k e^{ik(n-N/2)} b_k^\dagger \frac{1}{\sqrt{N}} \sum_p e^{-ip(n-N/2)} b_p | \text{GS} \rangle = \frac{1}{N} \sum_{k,p} e^{i(k-p)(n-N/2)} \langle \text{GS} | U_P^\dagger b_k^\dagger b_p U_P | \text{GS} \rangle. \tag{B13}$$

We must now calculate  $U_P^\dagger b_k^\dagger b_p U_P$  in the two-qubit case.

$$\begin{aligned}
 U_P^\dagger b_k^\dagger b_p U_P &= U_2^\dagger U_1^\dagger b_k^\dagger b_p U_1 U_2 \\
 &= U_2^\dagger U_1^\dagger [(b_k^\dagger [b_p, U_1] + [b_k^\dagger, U_1] b_p) + b_k^\dagger b_p] U_2 \\
 &= U_2^\dagger U_1^\dagger [(-\tilde{f}_p e^{ipx_1} \sigma_1^x b_k^\dagger U_1 - \tilde{f}_k e^{-ikx_1} \sigma_1^x U_1 b_p) + b_k^\dagger b_p] U_2 \\
 &= U_2^\dagger [(-\tilde{f}_p e^{ipx_1} \sigma_1^x) (-\tilde{f}_k e^{-ikx_1} \sigma_1^x) - \tilde{f}_p e^{ipx_1} \sigma_1^x b_k^\dagger - \tilde{f}_k e^{-ikx_1} \sigma_1^x b_p + b_k^\dagger b_p] U_2 \\
 &= U_2^\dagger (\tilde{f}_k \tilde{f}_p e^{-ikx_1} e^{ipx_1} - \tilde{f}_p e^{ipx_1} \sigma_1^x b_k^\dagger - \tilde{f}_k e^{-ikx_1} \sigma_1^x b_p + b_k^\dagger b_p) U_2 \\
 &= \tilde{f}_k \tilde{f}_p e^{-ikx_1} e^{ipx_1} + \tilde{f}_k \tilde{f}_p e^{-ikx_2} e^{ipx_2} - \tilde{f}_p e^{ipx_1} \sigma_1^x b_k^\dagger - \tilde{f}_k e^{-ikx_1} \sigma_1^x b_p - \tilde{f}_p e^{ipx_2} \sigma_2^x b_k^\dagger - \tilde{f}_k e^{-ikx_2} \sigma_2^x b_p + b_k^\dagger b_p \\
 &\quad + [-\tilde{f}_p e^{ipx_1} \sigma_1^x b_k^\dagger, U_2] + [-\tilde{f}_k e^{-ikx_1} \sigma_1^x b_p, U_2].
 \end{aligned}$$

The last two terms give

$$\begin{aligned} &= -\tilde{f}_p e^{ipx_1} \sigma_1^x (-\sigma_2^x \tilde{f}_k e^{-ikx_2}) - \tilde{f}_k e^{-ikx_1} \sigma_1^x (-\sigma_2^x \tilde{f}_p e^{ipx_2}) \\ &= \sigma_1^x \sigma_2^x \tilde{f}_p \tilde{f}_k e^{ipx_1} e^{-ikx_2} + \sigma_1^x \sigma_2^x \tilde{f}_p \tilde{f}_k e^{ipx_2} e^{-ikx_1}. \end{aligned}$$

Putting everything together, one has

$$\begin{aligned} U_p^\dagger b_k^\dagger b_p U_p &= \tilde{f}_k \tilde{f}_p e^{-ikx_1} e^{ipx_1} + \tilde{f}_k \tilde{f}_p e^{-ikx_2} e^{ipx_2} \\ &\quad - \sum_j \sigma_j^x (\tilde{f}_p e^{ipx_j} b_k^\dagger + \tilde{f}_k e^{-ikx_j} b_p) \\ &\quad + \sigma_1^x \sigma_2^x \tilde{f}_p \tilde{f}_k (e^{ipx_1} e^{-ikx_2} + e^{ipx_2} e^{-ikx_1}) \\ &\quad + b_k^\dagger b_p. \end{aligned} \quad (B14)$$

The ground state has no photons, so it only connects with itself through the first and second-to-last terms of  $U_p^\dagger b_k^\dagger b_p U_p$ . The first term connects the GS with itself completely, while the other cross connects the spin terms  $|00\rangle$  and  $|11\rangle$ . This yields

$$\begin{aligned} \langle \text{GS} | U_p^\dagger b_k^\dagger b_p U_p | \text{GS} \rangle &= \tilde{f}_k \tilde{f}_p e^{-ikx_1} e^{ipx_1} + \tilde{f}_k \tilde{f}_p e^{-ikx_2} e^{ipx_2} \\ &\quad + 2\alpha \beta \tilde{f}_p \tilde{f}_k (e^{ipx_1} e^{-ikx_2} + e^{ipx_2} e^{-ikx_1}). \end{aligned} \quad (B15)$$

Completing the Fourier transform, one finally arrives at

$$\langle b_n^\dagger b_n \rangle = |f_{n,1}|^2 + |f_{n,2}|^2 + 4\alpha\beta \text{Re} f_{n,1} f_{n,2}^*, \quad (B16)$$

where  $f_{n,1}$  is the Fourier transform of  $f_{k,1}$ , defined as

$$f_{k,1} = \tilde{f}_k e^{ikx_1}. \quad (B17)$$

### 6. Calculation of $\langle b_n^\dagger b_n \rangle$ for the bound states of the two-qubit scenario

The SEBS will be states of the form

$$|v\rangle = \beta_0 |01\rangle |0\rangle + \beta_1 |10\rangle |0\rangle + \sum_k \tilde{\beta}_k (\alpha |00\rangle + \beta |11\rangle) |1_k\rangle. \quad (B18)$$

Thus,

$$\begin{aligned} \langle b_n^\dagger b_n \rangle &= \langle v | b_n^\dagger b_n | v \rangle \\ &= \langle v | \frac{1}{\sqrt{N}} \sum_k e^{ik(n-N/2)} b_k^\dagger \frac{1}{\sqrt{N}} \sum_p e^{-ip(n-N/2)} b_p | v \rangle \\ &= \frac{1}{N} \sum_{k,p} e^{i(k-p)(n-N/2)} \langle v | U_p^\dagger b_k^\dagger b_p U_p | v \rangle. \end{aligned} \quad (B19)$$

We saw in Appendix B 5 that

$$\begin{aligned} U_p^\dagger b_k^\dagger b_p U_p &= \tilde{f}_k \tilde{f}_p e^{-ikx_1} e^{ipx_1} + \tilde{f}_k \tilde{f}_p e^{-ikx_2} e^{ipx_2} \\ &\quad - \sum_j \sigma_j^x (\tilde{f}_p e^{ipx_j} b_k^\dagger + \tilde{f}_k e^{-ikx_j} b_p) \\ &\quad + \sigma_1^x \sigma_2^x \tilde{f}_p \tilde{f}_k (e^{ipx_1} e^{-ikx_2} + e^{ipx_2} e^{-ikx_1}) \\ &\quad + b_k^\dagger b_p. \end{aligned} \quad (B20)$$

Contrary to what happened with the GS, all terms must now be considered because the SEBS connect through them all in one way or another. Thus, we must study each term individually.

The first two are trivial because they connect SEBS completely with themselves, so they will not be discussed.

The third term is more interesting. Through

$$- \sum_j \sigma_j^x (\tilde{f}_p e^{ipx_j} b_k^\dagger + \tilde{f}_k e^{-ikx_j} b_p), \quad (B21)$$

the term  $\beta_0 |01\rangle |0\rangle$  in  $|v\rangle$  becomes

$$-\beta_0 f_{p,1} |11\rangle |1_k\rangle - \beta_0 f_{p,2} |00\rangle |1_k\rangle, \quad (B22)$$

which connects with  $\tilde{\beta}_k (\alpha |00\rangle + \beta |11\rangle) |1_k\rangle$  to yield

$$-\beta_0 \tilde{\beta}_k (\beta f_{p,1} + \alpha f_{p,2}). \quad (B23)$$

The term  $\beta_1 |10\rangle |0\rangle$  in  $|v\rangle$  becomes

$$-\beta_1 f_{p,1} |11\rangle |1_k\rangle - \beta_1 f_{p,2} |00\rangle |1_k\rangle, \quad (B24)$$

which connects with  $\tilde{\beta}_k (\alpha |00\rangle + \beta |11\rangle) |1_k\rangle$  to yield

$$-\beta_1 \tilde{\beta}_k (\alpha f_{p,1} + \beta f_{p,2}). \quad (B25)$$

Naturally, the term  $(\alpha |00\rangle + \beta |11\rangle) \sum_k \tilde{\beta}_k |1_k\rangle$  connects with both  $\beta_0 |01\rangle |0\rangle$  and  $\beta_1 |10\rangle |0\rangle$  to yield the complex conjugate of the terms that we just calculated in the opposite direction.

Through the third term,

$$\sigma_1^x \sigma_2^x \tilde{f}_p \tilde{f}_k (e^{ipx_1} e^{-ikx_2} + e^{ipx_2} e^{-ikx_1}), \quad (B26)$$

the term  $\beta_0 |01\rangle |0\rangle$  in  $|v\rangle$  becomes

$$\beta_0 (f_{p,1} f_{k,2}^* + f_{p,2} f_{k,1}^*) |10\rangle |0\rangle, \quad (B27)$$

which connects with  $\beta_1 |10\rangle |0\rangle$  to yield

$$\beta_0 \beta_1 (f_{p,1} f_{k,2}^* + f_{p,2} f_{k,1}^*). \quad (B28)$$

Naturally, the term  $\beta_1 |10\rangle |0\rangle$  in  $|v\rangle$  becomes

$$\beta_1 (f_{p,1} f_{k,2}^* + f_{p,2} f_{k,1}^*) |01\rangle |0\rangle, \quad (29)$$

which connects with  $\beta_0 |01\rangle |0\rangle$  to yield

$$\beta_0 \beta_1 (f_{p,1} f_{k,2}^* + f_{p,2} f_{k,1}^*), \quad (B30)$$

the complex conjugate of its counterpart. Lastly, the term  $(\alpha |00\rangle + \beta |11\rangle) \sum_k \tilde{\beta}_k |1_k\rangle$  becomes

$$(\alpha |11\rangle + \beta |00\rangle) \sum_k \tilde{\beta}_k |1_k\rangle (f_{p,1} f_{k,2}^* + f_{p,2} f_{k,1}^*), \quad (B31)$$

and connects with  $(\alpha |00\rangle + \beta |11\rangle) \sum_k \tilde{\beta}_k |1_k\rangle$  to yield

$$2\alpha\beta (1 - \beta_0^2 - \beta_1^2) (\alpha |00\rangle + \beta |11\rangle) (f_{p,1} f_{k,2}^* + f_{p,2} f_{k,1}^*). \quad (B32)$$

Finally, the term  $b_k^\dagger b_p$  connects the  $p$ th and  $k$ th photonic terms to yield  $\tilde{\beta}_k^* \tilde{\beta}_k$ .

Summarizing, we have

$$\begin{aligned} \langle v | U_p^\dagger b_k^\dagger b_p U_p | v \rangle &= (f_{k,1}^* f_{p,2} + f_{k,2}^* f_{p,1}) - \beta_0 \tilde{\beta}_k (\beta f_{p,1} + \alpha f_{p,2}) \\ &\quad - \beta_1 \tilde{\beta}_k (\alpha f_{p,1} + \beta f_{p,2}) - \beta_0 \tilde{\beta}_k (\beta f_{k,1}^* + \alpha f_{k,2}^*) \\ &\quad - \beta_1 \tilde{\beta}_k (\alpha f_{k,1}^* + \beta f_{k,2}^*) + \beta_0 \beta_1 (f_{p,1} f_{k,2}^* + f_{p,2} f_{k,1}^*) \\ &\quad + 2\alpha\beta (1 - \beta_0^2 - \beta_1^2) (\alpha |00\rangle + \beta |11\rangle) \\ &\quad \times (f_{p,1} f_{k,2}^* + f_{p,2} f_{k,1}^*) + \tilde{\beta}_k^* \tilde{\beta}_k. \end{aligned} \quad (B33)$$

Completing the Fourier transform, one arrives at

$$\begin{aligned} \langle b_n^\dagger b_n \rangle &= |f_{n,1}|^2 + |f_{n,2}|^2 - 2\beta_0 \text{Re} \beta_n^* (\beta f_{n,1} + \alpha f_{n,2}) \\ &\quad - 2\beta_1 \text{Re} \beta_n^* (\alpha f_{n,1} + \beta f_{n,2}) + 4\beta_0 \beta_1 \text{Re} f_{n,1} f_{n,2}^* 4\alpha\beta \\ &\quad \times (1 - \beta_0^2 - \beta_1^2) \text{Re} f_{n,1} f_{n,2}^* + |\beta_n|^2, \end{aligned} \quad (\text{B34})$$

where  $f_{n,1}$  is the Fourier transform of  $f_{k,1}$ , defined as

$$f_{k,1} = \tilde{f}_k e^{ikx_1}. \quad (\text{B35})$$

### APPENDIX C: A GENERALIZED POLARON TRANSFORM

Let us consider a more general form of Eq. (2) for the two-qubit case, i.e.,  $N_q = 2$ :

$$\begin{aligned} H &= \frac{\epsilon}{2} \sum_{j=1}^2 \sigma_j^x + \frac{\Delta}{2} \sum_{j=1}^2 \sigma_j^z + \sum_k \omega_k b_k^\dagger b_k \\ &\quad + \sum_{j=1}^2 \sigma_j^x \sum_k c_k (b_k^\dagger e^{ikx_j} + \text{H.c.}), \end{aligned} \quad (\text{C1})$$

To accommodate the bias introduced to the qubits, we consider a variation of the polaron transform presented in Eq. (9)

$$U_P = \exp \left[ - \sum_{j=1}^2 \sigma_j^x \hat{\alpha}_j + \hat{\beta}_j \right], \quad (\text{C2})$$

with  $\hat{\alpha} = \sum_k \tilde{f}_k (b_k^\dagger e^{ikx_j} - b_k e^{-ikx_j})$  and  $\hat{\beta} = \sum_k \tilde{l}_k (b_k^\dagger e^{ikx_j} - b_k e^{-ikx_j})$ . When the new variational parameters  $\{\tilde{l}_k\}$  vanish, Eq. (C2) reduces to Eq. (9). In fact, provided there is no privileged direction of travel, so that  $|\tilde{f}_k| = |\tilde{f}_{-k}|$  and  $|\tilde{l}_k| = |\tilde{l}_{-k}|$ , and the fact that the sine is odd, it can be seen that the transform factors as

$$U_P = \bigotimes_{j=1}^2 U_j \tilde{U}_j, \quad (\text{C3})$$

with

$$U_j = \exp \left[ -\sigma_j^x \sum_k \tilde{f}_k (b_k^\dagger e^{ikx_j} - b_k e^{-ikx_j}) \right], \quad (\text{C4})$$

$$\tilde{U}_j = \exp \left[ \sum_k \tilde{l}_k (b_k^\dagger e^{ikx_j} - b_k e^{-ikx_j}) \right]. \quad (\text{C5})$$

Setting  $x_1 - x_2 = x$ , the minimization of the ground-state energy using this new transform yields the following spin mode:

$$\begin{aligned} \mathcal{H}_S &= \frac{\Delta_r}{2} (\sigma_1^z + \sigma_2^z) + \frac{\epsilon'}{2} (\sigma_1^x + \sigma_2^x) - \mathcal{J} \sigma_1^x \sigma_2^x \\ &\quad + 2 \sum_k \tilde{f}_k (\omega_k \tilde{f}_k - 2c_k) + 2 \sum_k \omega_k \tilde{l}_k^2 (1 + \cos kx), \end{aligned} \quad (\text{C6})$$

with

$$\epsilon' = \epsilon - 2 \sum_k \tilde{l}_k (c_k - \omega_k \tilde{f}_k) (1 - \cos kx). \quad (\text{C7})$$

This spin model is not exactly solvable, but performing perturbation theory on the term  $\frac{\epsilon'}{2} (\sigma_1^x + \sigma_2^x)$ , we find a ground-state energy of the form

$$\begin{aligned} \bar{E}_{\text{GS}} &= \frac{1}{2} (-\mathcal{J} - \mathcal{E} - \sqrt{(\mathcal{E} - \mathcal{J})^2 + 4\eta^2}) \\ &\quad + 2 \sum_k \tilde{f}_k (\omega_k \tilde{f}_k - 2c_k) + 2 \sum_k \omega_k \tilde{l}_k^2 (1 + \cos kx), \end{aligned} \quad (\text{C8})$$

where

$$\eta = \frac{\epsilon'}{\sqrt{2}} \frac{\Delta_r + \mathcal{E} + \mathcal{J}}{\sqrt{(\Delta_r + \mathcal{E})^2 + \mathcal{J}^2}}, \quad (\text{C9})$$

which is a minimum when

$$\tilde{l}_k = \frac{\eta}{\sqrt{2} \sqrt{(\mathcal{E} - \mathcal{J})^2 + 4\eta^2}} \frac{\Delta_r + \mathcal{E} + \mathcal{J}}{\sqrt{(\Delta_r + \mathcal{E})^2 + \mathcal{J}^2}} \frac{\omega_k \tilde{f}_k - c_k}{\omega_k}, \quad (\text{C10})$$

$$\tilde{f}_k = \frac{N_1 + N_2 + N_3 + N_4 + N_5}{D_1 + D_2 + D_3 + D_4 + D_5 + D_6 + D_7 + D_8}. \quad (\text{C11})$$

We have used the following compact notation to trim the lengthy expression of  $\tilde{f}_k$ :

$$N_1 = 4c_k + 2c_k \cos kx (1 + \mathcal{J}/\mathcal{E}), \quad (\text{C12})$$

$$N_2 = \frac{2c_k (1 + \cos kx) (\mathcal{E} + \mathcal{J} + \Delta_r)^2 \eta^2}{[(\Delta_r + \mathcal{E})^2 + \mathcal{J}^2][(\mathcal{E} - \mathcal{J})^2 + 4\eta^2]}, \quad (\text{C13})$$

$$N_3 = \frac{2c_k \cos kx (\mathcal{E} - \mathcal{J})(\mathcal{J}/\mathcal{E} - 1)}{\sqrt{(\mathcal{E} - \mathcal{J})^2 + 4\eta^2}}, \quad (\text{C14})$$

$$N_4 = \frac{8c_k \cos kx (1 + \mathcal{J}/\mathcal{E}) \eta^2}{(\mathcal{E} + \mathcal{J} + \Delta_r) \sqrt{(\mathcal{E} - \mathcal{J})^2 + 4\eta^2}}, \quad (\text{C15})$$

$$N_5 = \frac{8c_k \cos kx (2 + \Delta_r/\mathcal{E}) \eta^2 \mathcal{J}}{[\mathcal{J}^2 + (\mathcal{E} + \Delta_r)^2] \sqrt{(\mathcal{E} - \mathcal{J})^2 + 4\eta^2}}, \quad (\text{C16})$$

$$D_1 = 4\omega_k + 2\omega_k \cos kx (1 + \mathcal{J}/\mathcal{E}) + 2\Delta_r^2/\mathcal{E}, \quad (\text{C17})$$

$$D_2 = \frac{2\omega_k (1 + \cos kx) (\mathcal{E} + \mathcal{J} + \Delta_r)^2 \eta^2}{[(\Delta_r + \mathcal{E})^2 + \mathcal{J}^2][(\mathcal{E} - \mathcal{J})^2 + 4\eta^2]}, \quad (\text{C18})$$

$$D_3 = \frac{2\omega_k \cos kx (\mathcal{E} - \mathcal{J})(\mathcal{J}/\mathcal{E} - 1)}{\sqrt{(\mathcal{E} - \mathcal{J})^2 + 4\eta^2}}, \quad (\text{C19})$$

$$D_4 = \frac{2(\mathcal{E} - \mathcal{J}) \Delta_r^2}{\mathcal{E} \sqrt{(\mathcal{E} - \mathcal{J})^2 + 4\eta^2}}, \quad (\text{C20})$$

$$D_5 = \frac{8c_k \cos kx (1 + \mathcal{J}/\mathcal{E}) \eta^2}{(\mathcal{E} + \mathcal{J} + \Delta_r) \sqrt{(\mathcal{E} - \mathcal{J})^2 + 4\eta^2}}, \quad (\text{C21})$$

$$D_6 = \frac{8\Delta_r \eta^2 (1 + \Delta_r/\mathcal{E})}{(\mathcal{E} + \mathcal{J} + \Delta_r) \sqrt{(\mathcal{E} - \mathcal{J})^2 + 4\eta^2}}, \quad (\text{C22})$$

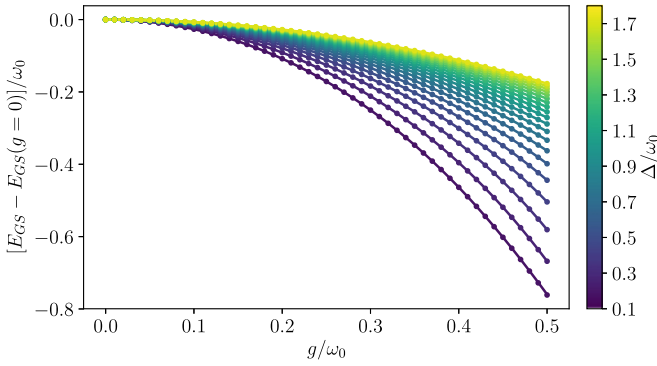


FIG. 14. Dependence of the ground-state energy on  $g$  for several values of  $\Delta$ , for  $x = 5$  and  $\epsilon = 10^{-4}$ . Solid lines represent results for the biased model. For comparison, dotted lines represent results for the unbiased model.

$$D_7 = \frac{8\omega_k \cos kx(2 + \Delta_r/\mathcal{E})\eta^2 \mathcal{J}}{[\mathcal{J}^2 + (\mathcal{E} + \Delta_r)^2] \sqrt{(\mathcal{E} - \mathcal{J})^2 + 4\eta^2}}, \quad (\text{C23})$$

$$D_8 = \frac{8\Delta_r \eta^2 (\mathcal{E} + \Delta_r)(1 + \Delta_r/\mathcal{E})}{[\mathcal{J}^2 + (\mathcal{E} + \Delta_r)^2] \sqrt{(\mathcal{E} - \mathcal{J})^2 + 4\eta^2}}. \quad (\text{C24})$$

As one can see, the calculations quickly become cumbersome when considering a biased model with the generalized polaron transform. At the same time, we find (see Fig. 14) that the results in frequency renormalization and ground-state energy do not deviate from those obtained with the standard transform in an unbiased model. That is why we have omitted this method in the main body of this paper. Nevertheless, it is important to notice that the introduction of a perturbative bias serves to lift the degeneracy between the ground state and the first-excited state of the effective spin model [Eq. (C6)] that arises when one goes beyond the USC regime into a scenario with full frequency renormalization, i.e.,  $\Delta_r \rightarrow 0$ .

#### APPENDIX D: CODE

All numerical calculations are available from Ref. [84].

- 
- [1] D. Roy, C. M. Wilson, and O. Firstenberg, *Rev. Mod. Phys.* **89**, 021001 (2017).
- [2] X. Gu, A. F. Kockum, A. Miranowicz, Y.-x. Liu, and F. Nori, *Phys. Rep.* **718**, 1 (2017).
- [3] O. Astafiev, A. M. Zagoskin, A. Abdumalikov, Y. A. Pashkin, T. Yamamoto, K. Inomata, Y. Nakamura, and J. Tsai, *Science* **327**, 840 (2010).
- [4] A. F. Van Loo, A. Fedorov, K. Lalumière, B. C. Sanders, A. Blais, and A. Wallraff, *Science* **342**, 1494 (2013).
- [5] Y. Liu and A. A. Houck, *Nat. Phys.* **13**, 48 (2017).
- [6] S. Faez, P. Türschmann, H. R. Haakh, S. Götzinger, and V. Sandoghdar, *Phys. Rev. Lett.* **113**, 213601 (2014).
- [7] P. Lodahl, S. Mahmoodian, and S. Stobbe, *Rev. Mod. Phys.* **87**, 347 (2015).
- [8] D. E. Chang, J. S. Douglas, A. González-Tudela, C.-L. Hung, and H. J. Kimble, *Rev. Mod. Phys.* **90**, 031002 (2018).
- [9] J. Argüello-Luengo, A. González-Tudela, T. Shi, P. Zoller, and J. I. Cirac, *Nature (London)* **574**, 215 (2019).
- [10] M. Bello, G. Platero, J. I. Cirac, and A. González-Tudela, *Sci. Adv.* **5**, eaaw0297 (2019).
- [11] P. Lodahl, S. Mahmoodian, S. Stobbe, A. Rauschenbeutel, P. Schneeweiss, J. Volz, H. Pichler, and P. Zoller, *Nature (London)* **541**, 473 (2017).
- [12] E. Sánchez-Burillo, C. Wan, D. Zueco, and A. González-Tudela, *Phys. Rev. Research* **2**, 023003 (2020).
- [13] H. Zheng, D. J. Gauthier, and H. U. Baranger, *Phys. Rev. Lett.* **111**, 090502 (2013).
- [14] T. Niemczyk, F. Deppe, H. Huebl, E. P. Menzel, F. Hocke, M. J. Schwarz, J. J. García-Ripoll, D. Zueco, T. Hümmer, E. Solano, A. Marx, and R. Gross, *Nat. Phys.* **6**, 772 (2010).
- [15] P. Forn-Díaz, J. Lisenfeld, D. Marcos, J. J. García-Ripoll, E. Solano, C. J. P. M. Harmans, and J. E. Mooij, *Phys. Rev. Lett.* **105**, 237001 (2010).
- [16] P. Forn-Díaz, J. J. García-Ripoll, B. Peropadre, J.-L. Orgiazzi, M. Yurtalan, R. Belyansky, C. M. Wilson, and A. Lupascu, *Nat. Phys.* **13**, 39 (2017).
- [17] J. P. Martínez, S. Léger, N. Gheeraert, R. Dassonneville, L. Planat, F. Foroughi, Y. Krupko, O. Buisson, C. Naud, W. Hasch-Guichard *et al.*, *npj Quantum Inf.* **5**, 19 (2019).
- [18] S. Léger, J. Puertas-Martínez, K. Bharadwaj, R. Dassonneville, J. Delaforce, F. Foroughi, V. Milchakov, L. Planat, O. Buisson, C. Naud, W. Hasch-Guichard, S. Florens, I. Snyman, and N. Roch, *Nat. Commun.* **10**, 5259 (2019).
- [19] J. H. Shirley, *Phys. Rev.* **138**, B979 (1965).
- [20] A. J. Leggett, S. Chakravarty, A. T. Dorsey, M. P. A. Fisher, A. Garg, and W. Zwerger, *Rev. Mod. Phys.* **59**, 1 (1987).
- [21] S. Ashhab and F. Nori, *Phys. Rev. A* **81**, 042311 (2010).
- [22] C. Ciuti, G. Bastard, and I. Carusotto, *Phys. Rev. B* **72**, 115303 (2005).
- [23] R. Stassi, A. Ridolfo, O. Di Stefano, M. J. Hartmann, and S. Savasta, *Phys. Rev. Lett.* **110**, 243601 (2013).
- [24] Q.-K. He, Z. An, H.-J. Song, and D. L. Zhou, *arXiv:1810.04523*.
- [25] S. D. Liberato, *Nat. Commun.* **8**, 1465 (2017).
- [26] R. Stassi, V. Macrì, A. F. Kockum, O. Di Stefano, A. Miranowicz, S. Savasta, and F. Nori, *Phys. Rev. A* **96**, 023818 (2017).
- [27] A. F. Kockum, A. Miranowicz, S. De Liberato, S. Savasta, and F. Nori, *Nat. Rev. Phys.* **1**, 19 (2019).
- [28] P. Forn-Díaz, L. Lamata, E. Rico, J. Kono, and E. Solano, *Rev. Mod. Phys.* **91**, 025005 (2019).
- [29] B. Peropadre, D. Zueco, D. Porras, and J. J. García-Ripoll, *Phys. Rev. Lett.* **111**, 243602 (2013).
- [30] T. Shi, Y. Chang, and J. J. García-Ripoll, *Phys. Rev. Lett.* **120**, 153602 (2018).
- [31] N. Gheeraert, X. H. H. Zhang, T. Sépulcre, S. Bera, N. Roch, H. U. Baranger, and S. Florens, *Phys. Rev. A* **98**, 043816 (2018).
- [32] E. Sanchez-Burillo, D. Zueco, J. J. Garcia-Ripoll, and L. Martin-Moreno, *Phys. Rev. Lett.* **113**, 263604 (2014).
- [33] E. Sánchez-Burillo, J. García-Ripoll, L. Martín-Moreno, and D. Zueco, *Faraday Discuss.* **178**, 335 (2015).

- [34] E. Sánchez-Burillo, L. Martín-Moreno, J. J. García-Ripoll, and D. Zueco, *Phys. Rev. Lett.* **123**, 013601 (2019).
- [35] D. Dzsotjan, J. Kästel, and M. Fleischhauer, *Phys. Rev. B* **84**, 075419 (2011).
- [36] A. González-Tudela, D. Martín-Cano, E. Moreno, L. Martín-Moreno, C. Tejedor, and F. J. García-Vidal, *Phys. Rev. Lett.* **106**, 020501 (2011).
- [37] D. Zueco, J. J. Mazo, E. Solano, and J. J. García-Ripoll, *Phys. Rev. B* **86**, 024503 (2012).
- [38] H. Zheng and H. U. Baranger, *Phys. Rev. Lett.* **110**, 113601 (2013).
- [39] M. T. Manzoni, L. Mathey, and D. E. Chang, *Nat. Commun.* **8**, 14696 (2017).
- [40] S. John, *Phys. Rev. Lett.* **53**, 2169 (1984).
- [41] S. John, *Phys. Rev. Lett.* **58**, 2486 (1987).
- [42] S. John and J. Wang, *Phys. Rev. Lett.* **64**, 2418 (1990).
- [43] S. John and J. Wang, *Phys. Rev. B* **43**, 12772 (1991).
- [44] S. John and T. Quang, *Phys. Rev. A* **50**, 1764 (1994).
- [45] A. González-Tudela, C.-L. Hung, D. E. Chang, J. I. Cirac, and H. J. Kimble, *Nat. Photonics* **9**, 320 (2015).
- [46] J. S. Douglas, H. Habibian, C.-L. Hung, A. V. Gorshkov, H. J. Kimble, and D. E. Chang, *Nat. Photonics* **9**, 326 (2015).
- [47] T. Shi, Y.-H. Wu, A. González-Tudela, and J. I. Cirac, *Phys. Rev. X* **6**, 021027 (2016).
- [48] G. Calajó, F. Ciccarello, D. Chang, and P. Rabl, *Phys. Rev. A* **93**, 033833 (2016).
- [49] A. González-Tudela and J. I. Cirac, *Phys. Rev. A* **96**, 043811 (2017).
- [50] A. González-Tudela and J. I. Cirac, *Phys. Rev. Lett.* **119**, 143602 (2017).
- [51] A. González-Tudela and J. I. Cirac, *Quantum* **2**, 97 (2018).
- [52] A. González-Tudela and J. I. Cirac, *Phys. Rev. A* **97**, 043831 (2018).
- [53] A. González-Tudela and F. Galve, *ACS Photonics* **6**, 221 (2018).
- [54] T. Shi, Y. H. Wu, A. González-Tudela, and J. I. Cirac, *New J. Phys.* **20**, 105005 (2018).
- [55] L. A. Khal'fin, *Sov. Phys.-JETP* **6**, 1053 (1958).
- [56] V. P. Bykov, *Sov. J. Quantum Electron.* **4**, 861 (1975).
- [57] L. Fonda, G. C. Ghirardi, and A. Rimini, *Rep. Prog. Phys.* **41**, 587 (1978).
- [58] D. S. Onley and A. Kumar, *Am. J. Phys.* **60**, 432 (1992).
- [59] B. Gaveau and L. Schulman, *J. Phys. A: Math. Gen.* **28**, 7359 (1995).
- [60] S. Garmon, H. Nakamura, N. Hatano, and T. Petrosky, *Phys. Rev. B* **80**, 115318 (2009).
- [61] S. Garmon, T. Petrosky, L. Simine, and D. Segal, *Fortschr. Phys.* **61**, 261 (2013).
- [62] S. Garmon, in *The Rochester Conferences on Coherence and Quantum Optics and the Quantum Information and Measurement Meeting* (OSA, Rochester, New York, 2013).
- [63] F. Lombardo, F. Ciccarello, and G. M. Palma, *Phys. Rev. A* **89**, 053826 (2014).
- [64] E. Sánchez-Burillo, D. Zueco, L. Martín-Moreno, and J. J. García-Ripoll, *Phys. Rev. A* **96**, 023831 (2017).
- [65] W. Ulrich, *Quantum Dissipative Systems (Second Edition)*, Series In Modern Condensed Matter Physics (World Scientific Publishing Company, Singapore, 1999).
- [66] J. Prior, A. W. Chin, S. F. Huelga, and M. B. Plenio, *Phys. Rev. Lett.* **105**, 050404 (2010).
- [67] M. Grifoni and P. Hänggi, *Phys. Rep.* **304**, 229 (1998).
- [68] K. Le Hur, *Understanding Quantum Phase Transitions* (CRC Press, Boca Raton, Florida, 2010), pp. 245–268.
- [69] R. Silbey and R. A. Harris, *J. Chem. Phys.* **80**, 2615 (1984).
- [70] S. Bera, A. Nazir, A. W. Chin, H. U. Baranger, and S. Florens, *Phys. Rev. B* **90**, 075110 (2014).
- [71] G. Díaz-Camacho, A. Bermudez, and J. J. García-Ripoll, *Phys. Rev. A* **93**, 043843 (2016).
- [72] D. Zueco and J. García-Ripoll, *Phys. Rev. A* **99**, 013807 (2019).
- [73] T. Shi, E. Demler, and J. I. Cirac, *Ann. Phys. (NY)* **390**, 245 (2018).
- [74] O. Di Stefano, A. Settineri, V. Macrì, L. Garziano, R. Stassi, S. Savasta, and F. Nori, *Nat. Phys.* **15**, 803 (2019).
- [75] D. P. S. McCutcheon, A. Nazir, S. Bose, and A. J. Fisher, *Phys. Rev. B* **81**, 235321 (2010).
- [76] H. Zheng, Z. Lü, and Y. Zhao, *Phys. Rev. E* **91**, 031003(R) (2015).
- [77] F. Guinea, E. Bascones, and M. Calderon, in *Lectures on the physics of highly correlated electron systems and high-Tc superconductors*, edited by F. Mancini, AIP Conf. Proc. No. 438 (AIP, New York, 1998), pp. 1–82.
- [78] H. Spohn and R. Dümcke, *J. Stat. Phys.* **41**, 389 (1985).
- [79] H. Löwen, *Phys. Rev. B* **37**, 8661 (1988).
- [80] L. Novotny and B. Hecht, *Principles of Nano-Optics* (Cambridge University Press, Padstow, UK, 2006).
- [81] P. Longo, P. Schmitteckert, and K. Busch, *Phys. Rev. Lett.* **104**, 023602 (2010).
- [82] P. Longo, P. Schmitteckert, and K. Busch, *Phys. Rev. A* **83**, 063828 (2011).
- [83] E. Sánchez-Burillo, A. Cadarso, L. Martín-Moreno, J. J. García-Ripoll, and D. Zueco, *New J. Phys.* **20**, 013017 (2018).
- [84] <https://github.com/chuan97/Bound-states-in-ultrastrong-waveguide-QED>.